On the promotional effect of Pd on the propene-assisted decomposition of NO on chlorinated Ce0.68 Zr0.32 O2

Cyril Thomas, Olivier Gorce, Céline Fontaine, Jean-Marc Krafft, Françoise Villain, Gérald Djéga-Mariadassou

On the promotional effect of Pd on the propene-assisted decomposition of NO on chlorinated $Ce_{0.68}Zr_{0.32}O_2$

Cyril Thomas*, Olivier Gorce[1], Céline Fontaine, Jean-Marc Krafft, Françoise Villain[2] and Gérald Djéga-Mariadassou

Laboratoire de Réactivité de Surface, UMR CNRS 7609, Université Pierre et Marie Curie, 4 Place Jussieu, Case 178, 75252 Paris cedex 05, France

[1]Present address: Renault sas, Centre Technique de Lardy, 1 allée Cornuel, 91510 Lardy, France

[2]Laboratoire de Chimie Inorganique et Matériaux Moléculaires, UMR CNRS 7071, Université Pierre et Marie Curie, 4 Place Jussieu, 75252 Paris cedex 05, France

Running title: C_3H_6-assisted decomposition of NO on $PdO_x/Ce_{0.68}Zr_{0.32}O_2$ catalysts

* To whom correspondence should be addressed:

Dr. Cyril Thomas

Laboratoire de Réactivité de Surface, UMR CNRS 7609, case 178, Université P. et M. Curie, 4 Place Jussieu 75252 Paris Cedex 05, France

e-mail: cthomas@ccr.jussieu.fr

Tel: + 33 1 44 27 36 30

Fax: + 33 1 44 27 60 33

Abstract:

The Selective Catalytic Reduction (SCR) of NO_x assisted by propene is investigated on $Pd/Ce_{0.68}Zr_{0.32}O_2$ catalysts (Pd/CZ), and is compared, under identical experimental conditions, with that found on a Pd/SiO_2 reference catalyst. Physico-chemical characterisation of the studied catalysts along with their catalytic properties indicate that Pd is not fully reduced to metallic Pd for the Pd/CZ catalysts. This study shows that the incorporation of Pd to CZ greatly promotes the reduction of NO in the presence of C_3H_6. These catalysts display very stable $deNO_x$ activity even in the presence of 1.7% water, the addition of which induces a reversible deactivation of about 10%. The much higher N_2 selectivity obtained on Pd/CZ suggests that the lean $deNO_x$ mechanism occurring on these catalysts is different from that occurring on Pd^0/SiO_2. A detailed mechanism is proposed for which CZ achieves both NO oxidation to NO_2 and NO decomposition to N_2, whereas PdO_x activates C_3H_6 via ad-NO_2 species, intermediately producing R-NO_x compounds that further decompose to NO and $C_xH_yO_z$. The role of the latter oxygenates is to reduce CZ to provide the catalytic sites responsible for NO decomposition. The proposed C_3H_6-assisted NO decomposition mechanism stresses the key role of NO_2, R-NO_x and $C_xH_yO_z$ as intermediates of the SCR of NO_x by hydrocarbons.

Key Words: CO-FTIR, XANES, Lean $deNO_x$, Mechanism, C_3H_6, Pd catalysts, Ceria-Zirconia, TPD of NO_x

1. Introduction

A tremendous number of investigations have been made within the past decades to develop catalysts capable of decreasing the emissions of air pollutants such as carbon monoxide (CO), hydrocarbons (HC) and nitrogen oxides (NO_x) from automotive gas exhausts [1-6]. The development of improved catalysts to meet the ever more stringent emissions standards is, however, still of key importance. To achieve this goal, the most promising means would obviously be to find a catalytic system that could directly decompose NO over a wide range of temperatures as pointed out by Pârvulescu et al. in a rather recent review [4]. Although a large number of catalysts have already been tested, no such system has as yet been found.

Three-Way Catalysts (TWC) were among the first possibilities investigated for lean NO_x abatement in car exhausts. These catalysts, which typically operate with an air-to-fuel ratio (A/F) close to the stoichiometry [1,5-7], are generally made up of a quite complicated combination of noble metals supported on an oxide carrier. These noble metals have shown to dissociate readily NO when present in their fully reduced state [1,2,4,8-10].

In addition to the ever more restricting limitations on carbon monoxide and nitrogen oxides, new regulations have appeared concerning the emission of carbon dioxide which is well known to be one of the greenhouse gases responsible for global warming. From this point of view, diesel engines, which operate typically under a lean mixture (air-to-fuel ratio (A/F) greater than unity), is among the solutions that must be considered to meet the CO_2 emission requirements. Indeed, such burning conditions lead to a lowering of fuel consumption and consequently to a decrease of the CO_2 emissions. Although these lean conditions have solved essentially the carbon monoxide and unburned hydrocarbon emission problems, they have made the classic TWC ineffective in removing nitrogen oxides from lean automotive gas exhausts.

The catalytic solution using a traditional TWC associated with a storage component (barium carbonate: $BaCO_3$) [11] which has been adopted for lean gasoline engines has still to be adapted for diesel cars which, as yet, have no suitable catalytic solution. A more attractive alternative would be to develop a specific catalyst capable of reducing nitrogen oxide emissions under lean conditions.

Among all the different formulations evaluated, to date, zeolite-based catalysts are probably those which have been studied most [3,4]. This might be due to the promising findings of Iwamoto et al. [12,13] and Lee and Armor [14] who showed that Cu-exchanged ZSM5 is able to decompose nitrogen monoxide at RT. This decomposition process is, however, self-inhibiting since as soon as nitrogen monoxide is decomposed on the catalytic sites (copper ions) they are poisoned by the oxygen left from nitrogen monoxide decomposition and, thus, the reaction stops. It is important to notice the striking similarity with model TWC reported in the case of stoichiometric mixture by Djéga-Mariadassou and co-workers [7,15,16]. These authors demonstrated the competition between the CO oxidation reaction and the assisted decomposition of NO by CO. In lean exhausts, carbon monoxide cannot be further used to assist the decomposition of nitrogen monoxide [16]. Consequently, other reductants such as hydrocarbons must be used to assist the decomposition of nitrogen monoxide. In the case of model exhausts, it has been shown by Matsumoto et al. [17] that alkenes, and more particularly propene, are the most efficient reductants to assist the nitrogen monoxide reduction. Alkenes are, however, also known as coke precursors for acidic catalysts which accounts for the dramatic deactivation of zeolite-based catalysts when propene is present in the lean mixture [18]. In addition to this coking phenomenon, zeolite-based catalysts are rather sensitive to water, and deactivation was also reported due to their low hydrothermal resistance [4]. These drawbacks have led researchers to focus on oxides-supported Platinum Group Metals (PGMs) catalysts. Due to their intrinsic higher activity [19-

21], supported Pt catalysts have been the subject of the greatest number of studies [9,22-33]. These are followed by supported Rh [10,19-21,33] and Pd [19-21,33,34] catalysts. Although these catalysts exhibit significant lean deNO_x activity with C_3H_6 as reductant and quite reasonable stability, they have a rather narrow temperature operating window [19] and fairly poor selectivity to N_2 [9,30,34,35]. N_2O, which is well known as a component of the greenhouse effect [36], is, indeed, formed in substantial amounts. High selectivity to N_2 has, however, been reported for Rh/Al_2O_3 catalysts [10,19,33]. Alumina-supported Rh catalysts usually operate at much higher temperatures than either supported Pt or Pd catalysts. This peculiarity led Obuchi et al. to the conclusion that this high selectivity to N_2 was attributable to an additional catalytic effect of the alumina support [33]. The influence of the nature of the support was also investigated [19,20,30]. These studies, however, did not report on PGMs supported on ceria-zirconia (CZ) until recently for Rh/CZ [37] or Pt catalysts supported on CZ-Al_2O_3 [31] and pure CZ [32]. Finally, CZ showed only very moderate lean deNO_x activity in the presence of C_3H_6 [38].

The aim of this work is to investigate the influence of Pd addition to a chlorinated ceria-zirconia support on lean deNO_x with C_3H_6 as reductant. To our knowledge, such catalysts have not been investigated for this particular reaction. They have, however, been widely studied in the fields of TWC [39-43], CH_4 total oxidation [44,45] and hydrocarbon reforming [46]. For comparison, the performances of a Pd/SiO_2 catalyst are also reported. Pd/CZ catalysts show enhanced lean deNO_x activity and much higher N_2 selectivity compared to Pd/SiO_2. This suggests the involvement of distinct lean deNO_x reaction mechanisms within these two catalytic systems. Based on transient and steady-state experiments, a mechanism of the lean deNO_x is proposed for the Pd/CZ catalysts.

2. Experimental

2.1. Catalyst synthesis

2.1.1. Ceria-zirconia ($Ce_{0.68}Zr_{0.32}O_2$: CZ)

The CZ solid solution was provided by Rhodia. The CZ was added to chloridric acid solution (pH 1.9) prepared by adding HCl to distilled water. After ageing for 2 hours under vigorous stirring, CZ was filtered and washed with distilled water before being dried in air at 120°C for 3 hours.

2.1.2. Pd/CZ

Two ceria-zirconia-supported Pd catalysts (0.54 and 0.89 wt% Pd) were prepared by incipient wetness impregnation of the chlorinated support by an aqueous solution of $PdCl_2$, $3H_2O$ (Johnson Matthey). After impregnation, the catalysts were aged for 2 hours and dried in air at 120°C for three hours.

2.1.3. Pd/SiO_2

For comparison with Pd/CZ catalysts, a silica (Degussa, Aerosil 50)-supported palladium catalyst (0.93 wt% Pd) was prepared by incipient wetness impregnation of the support by an aqueous solution of $PdCl_2$, 3 H_2O (Johnson Matthey). After impregnation, the catalyst was aged for 2 hours and dried in air at 120°C for three hours.

2.2. Catalyst characterization

Metal and chlorine contents were determined by chemical analyses (CNRS – Vernaison). The chlorine content was about 1 wt% for the CZ-based catalysts before and after reaction.

The specific surface areas were determined by physisorption of N_2 at 77K using a Quantasorb Jr. dynamic system equipped with a thermal conductivity detector (TCD). The specific surface areas were calculated using the BET method. For CZ-supported catalysts, the specific surface areas were about 100 $m^2\ g^{-1}$ before and after testing, whereas that of Pd/SiO_2 was about 50 $m^2\ g^{-1}$.

2.2.1 Determination of the percentage of exposed zero-valent Pd atom (PEM^0)

With the well-known reducibility of the CZ support [47], the determination of the percentage of exposed zero-valent Pd atom was done by means of propene hydrogenation [48].

Prior to propene hydrogenation, the catalyst sample (30-60 mg deposited on sintered glass of a pyrex reactor) was heated in flowing H_2 (100 $mL_{NTP}\ min^{-1}$) at atmospheric pressure with a heating rate of 3°C min^{-1} up to 300°C and was kept at this temperature for 2h. After cooling to –78°C under H_2, the reaction was started. The partial pressure of propene was 51.8 torr, and the total flow rate was 107 $mL_{NTP}\ min^{-1}$ with H_2 as balance.

The composition of the effluents was analyzed by means of an on-line gas chromatograph (Hewlett Packard 5890, FID) equipped with a CP-Al_2O_3/KCl (Chrompack, 50 m long, 0.32 mm inner diameter, 5 µm film thickness) capillary column. The only detected product was propane.

From the initial reaction rates obtained, the numbers of exposed zero-valent Pd atoms were calculated according to a turnover rate of 0.40 s^{-1} for the propene hydrogenation reaction at -78°C [48].

2.2.2. Temperature-Programmed Reduction

Temperature-Programmed Reduction (TPR) experiments were performed in a conventional system equipped with a thermal conductivity detector. After calcination at 500°C for 2h, the reduction was carried out in a flow of H_2 (5%) in Ar (25 mL min^{-1}) using a heating rate of 5°C min^{-1}. Typically, the reduction was carried out up to 700°C and then the sample (0.02-0.05 g) was kept at this temperature for 15 min. H_2O evolving in the course of the TPR experiments was trapped by a 5A molecular sieve. The amount of H_2 uptake in the TPR was estimated from integrated peak areas.

2.2.3. X-Ray diffraction

X-Ray diffraction (XRD) patterns of CZ, SiO_2, Pd(0.93)/SiO_2 and Pd/CZ were obtained on a SIEMENS D500 diffractometer with a Cu K_α monochromatized radiation.

2.2.4. X-ray absorption near edge spectroscopy (XANES)

X-Ray absorption measurements were carried out using synchrotron radiation of the XAS13 station at LURE (Orsay, France) on line D42 (May 3-4, 2001). Fluorescence yield spectra of Pd(0.54)/CZ were recorded at RT using a Ge solid detector (Eurisys, 7 elements) combined with a multichannel analyser to select the Pd Kα fluorescence, whereas those of the reference compounds (Pd foils, 20 µm thick, PdO (> 99% pure, Lancaster)) were collected in the transmission mode. The incident beam was monochromatized using a Ge (400) double monochromator. XANES spectra were collected at the Pd K edge with a sampling step of 2.0 eV/point from 24300 to 24500 eV and an integration time of 10s and 2s in fluorescence and transmission modes, respectively. The energy was calibrated using the Pd foil. XANES spectra were obtained from Pd(0.54)/CZ either after oxidation or reduction treatments under flowing air or H_2 (100 mL_{NTP} min^{-1}) for 2h at 500°C. To avoid the exposure of the reduced

sample to O_2, the catalyst was then transferred into a UV cell (Suprasil quartz, 5 cm long, 1cm wide and 1 cm high) that was finally sealed under vacuum ($5x10^{-5}$ torr). In the case of the oxidized sample, we checked that the high purity silica glass did not interfere with incident and fluorescent beams. Superimposed spectra were, indeed, obtained with this sample located either into the UV cell or between Kapton tapes. The cell was set to 45° with respect to the incident RX beam and the fluorescence detector. The extraction of the data was done with Michalowicz's software package [49,50].

2.2.5. Fourrier transform infra-red spectroscopy

Fourrier transform infra-red (FTIR) spectra of adsorbed CO on CZ and Pd(0.89)/CZ were collected on a Bruker Vector 22 FTIR spectrometer equipped with a liquid N_2-cooled MCT detector and a data acquisition station. 256 scans were averaged with a spectral resolution of 2 cm^{-1}.

The samples were pressed into self-supporting wafers of 6-11 mg cm^{-2}. The wafers were loaded in a moveable glass sample holder, equipped on top with an iron magnet, inserted in a conventional pyrex-glass cell (CaF_2 windows) connected to a vacuum system. The iron magnet allowed the transfer of the catalyst sample from the oven-heated region to the infrared light beam.

Prior to adsorption of CO, the catalysts were submitted to a dynamic (50 cm^3 min^{-1}) reducing pretreatment (5% H_2 in Ar, Air Liquide, 99.999%) at 500°C for 2 h at atmospheric pressure. The catalyst samples were then evacuated (10^{-6} mbar) at 500°C for 60 min before the temperature was decreased to RT under dynamic vacuum.

CO (Air Liquide, 99.999%), trapped at 77 K, was adsorbed at RT at equilibrated pressures of 0.9 and 18 torr.

The spectrum of the pretreated catalyst was used as reference and subtracted from the spectra of the catalyst exposed to CO.

2.3. Catalytic runs

Prior to catalytic runs, the samples were calcined in situ in dry air at 500°C (4°C.min^{-1}) for 2 hours with a flow rate of 500 mL_{NTP} min^{-1} per gram of catalyst.

Steady-state, Temperature-Programmed Desorption (TPD) and Temperature-Programmed Surface Reaction (TPSR) experiments and were carried out. After being contacted with the appropriate gas mixture at RT, temperature transient experiments were carried out from RT to 500°C with a heating rate of 10°C min^{-1}. Before the TPD experiments, the catalyst samples were flushed in N_2 to remove RT physisorbed species from the adsorption mixture.

The experiments were carried out in a U-type quartz reactor. The sample (0.2 g unless otherwise specified) was held between plugs of quartz wool, and the temperature was controlled through a WEST 4000 temperature controller using a K type thermocouple. Reactant gases were fed from independent mass flow controllers (Brooks 5850E). The total flow was 250 mL_{NTP} min^{-1} to which corresponds a HSV (Hour Space Velocity) of 112,500 h^{-1}.

Catalytic experiments were carried out with C_3H_6 as reductant. Typically, the composition of the C_3H_6-NO-O_2 reacting mixture was: 1900 ppm C_3H_6, 340 ppm NO and 8% O_2 in N_2. The reactants, diluted in N_2, were fed from independent gas cylinders (Air Liquide).

The reactor outflow was continuously analysed using the combination of four different detectors. An Eco Physics CLD 700 AL chemiluminescence NO_x analyser (for NO and total NO_x (*i.e.* NO + NO_2)) allowed the simultaneous detection of both NO and NO_x. Two Ultramat 6 IR analysers were used to monitor N_2O, CO and CO_2. A FID detector (Fidamat 5A) was

used to follow the concentration of hydrocarbons. We checked that, under our experimental conditions, CO and CO_2 had a negligible response on the N_2O IR analyser, whereas that of C_3H_6 was significant. C_3H_6 contribution to the N_2O signal was taken into account to calculate the "true" N_2O concentration ($[N_2O]$) as follows (Eq. 1):

$$[N_2O] = [N_2O]_{meas.} - \frac{[N_2O]^0 \text{ x } [C_3H_6]_{meas.}}{[C_3H_6]_{inlet}} \quad (1)$$

where $[N_2O]^0$, $[C_3H_6]_{inlet}$, $[C_3H_6]_{meas.}$ and $[N_2O]_{meas.}$ are: the concentrations of N_2O due to the contribution of the inlet concentration of C_3H_6, the inlet concentration of C_3H_6, C_3H_6 and N_2O concentrations measured in the course of the reaction, respectively. As N_2 was used as balance, the conversion of NO_x to N_2 was calculated assuming 100% nitrogen mass balance (Eq. 2):

$$\text{Conversion of } NO_x \text{ to } N_2 \,(\%) = \frac{[NO_x]_{inlet} - ([NO_x]_{outlet} + 2\,x\,[N_2O])}{[NO_x]_{inlet}} \quad (2)$$

where $[NO_x]_{inlet}$ and $[NO_x]_{outlet}$ are the concentrations of NO_x at the inlet and at the outlet of the reactor, respectively.

In one experiment, over $Ce_{0.68}Zr_{0.32}O_2$, propene was substituted by 1-propanol (Merck, spectroscopic grade) with a concentration of 2200 ppm by means of a saturator.

3. Results

3.1. Catalyst characterization

3.1.1. Determination of the percentage of exposed zero-valent metal atoms (PEM^0)

Table 1 lists the percentage of exposed zero-valent palladium atoms of the CZ-supported Pd catalysts and $Pd(0.93)/SiO_2$. The percentage of exposed zero-valent Pd atoms is about 17 and 22% for Pd/CZ and $Pd(0.93)/SiO_2$, respectively.

3.1.2. TPR results

Fig. 1 shows the TPR profiles of the calcined catalysts. For Pd(0.93)/SiO_2, the trace of which is magnified by a factor of 4 for the sake of clarity, a reduction peak is observed at about 50°C.

For the CZ sample, the trace of which is magnified by a factor of 3, a broad reduction peak starting around 400°C and ranging to a maximum at 530°C is observed. This reduction temperature region corresponds well with that reported for various ceria-zirconia materials [51-55].

The presence of noble metal on CZ modifies substantially the features of the TPD profiles. Indeed, the reduction peak revealed over the CZ sample vanishes, while a strong signal appears at temperatures below 200°C depending on the catalyst sample. It is observed that the reduction peak shifts to lower temperature with increasing Pd content. Luo and Zheng [56] reported a similar feature despite the fact that their TPR traces were substantially different from ours.

As it is well established that the incorporation of noble metals increases the reducibility of the ceria-related materials [47,51,52,56,57], quantitative analysis of the TPR traces is not discussed. Overall, the amount of H_2 consumed in the course of the TPR was close to 0.5 10^{-3} mol g^{-1} for all samples. This value agrees well with those listed by Luo and Zheng for $Ce_{0.5}Zr_{0.5}O_2$-supported Pd catalysts [56].

Finally, the comparison of the TPR traces of Pd(0.93)/SiO_2 and Pd(0.89)/CZ clearly shows that the Pd species interact to a greater extent with CZ than with SiO_2. The reduction peak of these Pd species supported on CZ is, indeed, shifted to higher temperature compared with that of Pd(0.93)/SiO_2.

3.1.3. XRD

XRD patterns of the calcined SiO_2, Pd(0.93)/SiO_2 and CZ samples are shown in Fig. 2. After calcination of Pd(0.93)/SiO_2, a diffraction peak is observed at about 33.8° which corresponds to PdO (101 plane). Two very weak peaks at about 41.9 and 54.8° can also be assigned to PdO. As shown in Fig. 2, the diffraction pattern of CZ exhibits 4 peaks at about 29, 33.8, 48.3 and 57.2°. Owing to the weak intensity of the PdO peaks and the overlapping with CZ support, the presence of PdO on the CZ-supported catalysts could not be established through XRD.

3.1.4. XANES measurements

XANES spectra of the Pd(0.54) catalyst after calcination or reduction are shown in Fig. 3. The shape of the XANES spectra of the Pd(0.54)/CZ sample either calcined (----) or reduced (—) corresponds fairly well to that of the PdO (▲) and Pd metal (Δ) references (Fig. 3), respectively. This result markedly differs from that of the reduced Rh/CZ catalyst, which showed a XANES spectrum different from both Rh foil and Rh_2O_3 references [58].

3.1.5. IR

The CO-FTIR technique was used to probe the nature of the metal species [59] supported on CZ.

The FTIR spectra of adsorbed CO under equilibrated pressures of 0.9 and 18 torr of CO are shown in Fig. 4 for CZ and Pd(0.89)/CZ. It is worthwhile noting the fairly low intensity of the CO absorption bands. This is why the CO-FTIR of the Pd(0.54)/CZ catalyst was not investigated.

Over CZ (Fig. 4a), two CO absorption bands are observed at 1575 and 2167 cm^{-1}. The band at 1575 cm^{-1} can be assigned to the formation of carbonates [60]. This band appears as

soon as the equilibrated pressure of CO is 0.9 torr, whereas the band at 2167 cm^{-1} is observed only at a pressure of 18 torr. This latter band has been attributed to the weak interaction of CO with Ce surface sites [61-64].

The FTIR spectra of adsorbed CO on Pd(0.89)/CZ (Fig. 4b) differ markedly from those of CZ. The formation of carbonate is not observed, and a rather broad absorption band from 1850 to 2090 cm^{-1} is revealed, with two maxima at 1950 and 2083 cm^{-1}. The band at 1950 cm^{-1}, also found in a previous work of Badri et al. on a chlorinated Pd/CeO_2 sample [61], can be assigned to bridged CO species bonded to zero-valent Pd atoms ($Pd^0{}_2CO$) [43,65,66]. In contrast, the band with the maximum at 2083 cm^{-1} corresponds to CO species singly bonded to Pd^0 atoms [43,59,61,63,65]. CO coordinated to Ce^{z+} centers, acting as Lewis acid sites, gives rise to an absorption band at 2175 cm^{-1}, as already reported by Badri et al. [61].

3.1.6. NO oxidation

As reported earlier [38 and references therein], the oxidation of NO to NO_2 is suspected to be an essential step of the deNO_x process. This reaction was, thus, investigated over CZ and Pd(0.54)/CZ under steady-state conditions. As shown in Fig. 5, NO oxidation is the greatest at 400°C. At higher temperatures, the conversion of NO decreases due to thermodynamic limitations. It is important to note that the addition of Pd does not promote NO oxidation, and this reaction is only catalysed by the CZ support.

3.1.7. Adsorption of NO-O_2 – TPD in N_2

Fig. 6 shows the NO_x TPD profiles in N_2 of samples contacted with NO-O_2 (340 ppm-8%). The addition of Pd to CZ does not affect the TPD profiles to a large extent. In both cases, two NO peaks are observed at about 100 and 420°C, and a broad NO_2 desorption

profile is seen from 50 to 450°C. This NO_2 feature exhibits two maxima at low and high temperatures. The high temperature maximum is close to 350°C and is not affected by the introduction of Pd. In contrast, the low temperature maximum shifts from 116 to 136°C when Pd is added to CZ (Fig. 6c). For both samples, the quantities of adsorbed and desorbed NO_x closely match (Table 2). Table 2 shows that the amount of adsorbed NO_x fluctuates to some extent. This was related to slightly different times of exposure and not to differences in the starting conditions of the samples. In agreement with previous work [67], PdO/SiO_2 did not chemisorb NO_x. Consequently, the TPD in C_3H_6-O_2 after NO_x chemisorption was not performed.

3.1.8. Adsorption of NO-O_2 – TPD in C_3H_6-O_2

After exposure of the samples to a NO-O_2 mixture, the TPD profiles obtained in C_3H_6-O_2 are shown in Fig. 7 for CZ and Pd(0.89)/CZ. Before TPD, the samples were flushed by N_2 to remove physisorbed NO_x and then contacted with the desorption gas mixture (C_3H_6-O_2) for a few minutes at RT. For both samples, a C_3H_6 desorption profile is observed at low temperature. It is worth mentioning that in the case of the oxidation of C_3H_6 by O_2 without pre-adsorption of NO_x (not shown), a similar desorption feature was observed. This low temperature desorption feature is, thus, attributed to propene species chemisorbed on catalytic sites different from those occupied by adsorbed NO_x species. For both catalysts, HC consumption starts at 80°C and a more drastic HC consumption is observed at about 110°C. It is worthwhile mentioning that the HC consumption profile is slightly different for Pd(0.89)/CZ compared with that of CZ. At temperatures higher than 150°C, the HC concentration reaches its input concentration for CZ (Fig. 7a). This phenomenon, however, is not observed for Pd(0.89)/CZ (Fig. 7b). The first column of Table 3 shows that the light-off

temperature of C_3H_6 in the course of the TPD in C_3H_6-O_2 decreases drastically with the addition of Pd.

Considering desorption of the N_tO_x (NO, NO_2 and N_2O) species, rather complicated profiles are observed (Fig. 7). A detailed description of the traces seen for CZ is reported in a recent article [38]. The amounts of adsorbed and desorbed N_tO_x species are listed in Table 2. For both catalysts, a comparison of the desorbed quantities (Table 2) and profiles of N_tO_x species of the two TPD experiments either in N_2 (Fig. 6) or in C_3H_6-O_2 (Fig. 7) after exposure of the samples to NO-O_2 shows striking differences. First, NO becomes the major N_tO_x species of the TPD in C_3H_6-O_2. In contrast, NO_2 is the major species of the TPD in N_2. Second, the global amount of desorbed N_tO_x species, taking into account that N_2O originates from the recombination of two NO_x molecules, is always lower than that adsorbed for the TPD in C_3H_6-O_2. On the other hand, adsorbed and desorbed NO_x quantities agree well for the TPD in N_2. These results suggest that part of the adsorbed NO_x is reduced to N_2 in the presence of C_3H_6 in the desorption mixture. Finally, the N_tO_x TPD profiles (Fig. 7) suggest that part of the adsorbed NO_x species reacted with C_3H_6 in the low temperature region (50-115°C). For N_tO_x species, the NO_x desorption feature is clearly truncated in this low temperature region compared to that of the TPD in N_2 (Fig. 6). As already discussed [38], these concomitant consumptions suggest the interaction of adsorbed NO_x species (ad-NO_x) with propene and the formation of mixed compounds (R-NO_x) stored on the catalytic material. For Pd(0.89)/CZ, it is worth adding that a stabilised HC consumption occurs up to higher temperatures, ca. 150°C, compared with that observed on CZ (Fig. 7). Overall, the broad N_tO_x desorption features observed at low temperatures (100-200°C) over CZ become thinner over Pd(0.89)/CZ, whereas those at high temperatures (220-400°C) are clearly shifted to lower temperatures (200-300°C) with the incorporation of Pd. In addition, the amount of

NO_2 desorbed at temperatures higher than 200°C is much lower over Pd(0.89)/CZ than over CZ. That of N_2O is, however, greater.

3.1.9. C_3H_6 oxidation by O_2

Fig. 8 shows that the C_3H_6 oxidation profiles are obviously different depending on the nature of the catalyst support.

On Pd(0.89)/CZ, C_3H_6 oxidation is rather similar to that observed after adsorption of $NO-O_2$ (Fig. 7b) with comparable light-off temperature (Table 3). On such a catalyst, however, the consumption of C_3H_6 in the $C_3H_6-O_2$ reaction starts at a higher temperature and is more pronounced before 250°C than after adsorption of $NO-O_2$. In contrast, C_3H_6 oxidation proceeds much more steeply in a much narrower range of temperature (from 195 to 260°C) on Pd(0.93)/SiO_2 than on Pd(0.89)/CZ (Fig. 8). In addition, C_3H_6 does not chemisorb at RT on Pd(0.93)/SiO_2, as is the case of Pd(0.89)/CZ that shows a low temperature C_3H_6 desorption feature. For Pd(0.93)/SiO_2, it is worthwhile noting that the experiment reported on Fig. 8 was carried out after a previous C_3H_6-$NO-O_2$ Temperature-Programmed Surface Reaction (TPSR). It will be shown later (please refer to part 3.1.10.) that for Pd(0.93)/SiO_2 such an experimental sequence does significantly influence the light-off temperature of C_3H_6, whereas it has no impact on CZ-supported catalysts.

Table 3 shows that the C_3H_6 light-off temperature for the $C_3H_6-O_2$ reaction is the lowest for Pd(0.93)/SiO_2 and the highest for CZ. Finally, Pd promotes significantly C_3H_6 oxidation for the CZ-based catalysts.

3.1.10. C_3H_6-$NO-O_2$ TPSR experiment

TPSR of the complete reacting mixture was performed after exposure of Pd(0.89)/CZ to the reacting mixture at RT (Fig. 9). The features observed are comparable to those seen for

the TPD in C_3H_6-O_2 after adsorption of NO-O_2 (Fig. 7b). NO desorption is the major N_tO_x species with a two peak profile (100 and 220°C). The formation of NO_2 and N_2O are, however, more limited than those obtained for the TPD experiment in C_3H_6-O_2 (Fig. 7). C_3H_6 and NO_x consumptions detected in the low temperature region in the case of the TPD experiment in C_3H_6-O_2 are no longer observed. C_3H_6 is moderately consumed from 100 to 200°C and at higher temperatures the oxidation of C_3H_6 accelerates. More interesting is that the NO_x profile shows a decrease of the NO_x concentration at 297°C corresponding to 50% of the NO_x inlet concentration. At this temperature, the conversion of C_3H_6 is 79%. At higher temperatures, the NO_x concentration reaches back its inlet concentration, and NO is oxidized to NO_2 when full conversion of C_3H_6 is achieved at about 400°C.

Compared with the TPSR profiles found on CZ (Fig. 12 of [38]), the desorption peak of NO reported in this experiment at about 300°C is no longer observed in the course of the TPSR on Pd(0.89)/CZ, as a NO_x deficit occurs in this temperature range (Fig. 9).

The TPSR profiles of Pd(0.93)/SiO_2 (not shown) are less complicated than those of Pd(0.89)/CZ. The most interesting peculiarity is that if the temperature is decreased from 500°C to RT (reverse TPSR) after the first TPSR experiment, the C_3H_6 light-off temperature and the selectivity to N_2 are modified significantly. The C_3H_6 light-off temperature and the N_2 selectivity of the TPSR and the reverse TPSR decrease from 298 to 237°C (Table 3) and from 70 to 30%, respectively. On the other hand, the conversion of NO_x to N_2 remains almost constant and close to 9% at maximum NO_x conversion.

Such phenomena were not observed for the CZ-based catalysts for which the C_3H_6 and NO_x profiles of the TPSR and the reverse TPSR were comparable.

As in the case of the C_3H_6-O_2 reaction, Table 3 shows that the C_3H_6 light-off temperature for the TPSR is lowest for Pd(0.93)/SiO_2 and highest for CZ. Pd also promotes significantly C_3H_6 oxidation for the CZ-based catalysts.

3.1.11. Steady-state NO-C_3H_6-O_2 reaction

Prior to steady-state measurements, the catalysts were submitted to a TPSR under the complete reacting mixture from RT to 500°C with a heating rate of 10°C min^{-1}.

Fig. 10 shows the performances of the catalysts for the reduction of NO_x under steady-state conditions with stepwise increase of the temperature. The temperature of maximum of N_2 formation, the corresponding NO_x and C_3H_6 conversions are listed in Table 4.

It is obvious that the introduction of Pd leads to a significant increase of NO_x reduction to N_2 as well as a drastic decrease of the C_3H_6 light-off temperature. Table 3 lists the temperature of light-off of C_3H_6 over various Pd-containing catalysts with respect to reaction conditions. From this table it can also be concluded that the presence of NO does not influence this light-off temperature, as was the case for CZ ([38] and first line of Table 3).

Conversion of NO_x to N_2 higher than 20% is obtained on the Pd/CZ catalysts. On the other hand, Pd(0.93)/SiO_2 shows a rather low conversion of NO_x to N_2 close to that found for CZ, despite the fact that the light-off temperature of propene is similar to that of the most active CZ-based catalyst (Pd(0.89)/CZ). One also may note that propene oxidation is steeper over Pd(0.93)/SiO_2 than over Pd/CZ catalysts. It is worthwhile noting that N_2 selectivity is higher than 80% on CZ-based catalysts, whereas that of Pd(0.93)/SiO_2 is of 28% (Table 4). Finally, Fig. 10e shows that NO oxidation to NO_2 is almost eliminated in the presence of C_3H_6 before 400°C, the temperature of which corresponds to the almost complete conversion of C_3H_6 (Fig. 10c).

To illustrate the high stability of the CZ-supported catalysts, Table 5 reports on the influence of time on stream on the reduction of NO_x on Pd(0.89)/CZ. This catalyst exhibits NO_x conversion to N_2 by about 30% and does not deactivate in the absence of water for 1 h. After about 1 hour of run, 1.7% of water was introduced in the reaction mixture. This addition decreases the conversion of NO_x by about 10%. More interesting is that the catalyst does not

deactivate over a period of 19 hours on stream in the presence of water. After 19 hours on stream, the initial activity is restored when water is removed from the feed. This suggests that H_2O competes with the active sites responsible for N_2 formation. C_3H_6 conversion remains almost unaffected and close to 60%. Chemical analysis of this sample after reaction reveals a carbon content of only 0.4 wt%.

3.1.12. Steady-state NO-C_3H_6-O_2 reaction over mechanical mixtures

The results obtained over two mechanical mixtures of Pd(0.89)/CZ + SiO_2 and Pd(0.93)/ SiO_2 + CZ are shown in Fig. 11. It is obvious that the mechanical mixture of Pd(0.89)/CZ + SiO_2 (Fig. 11a) is more active than its counterpart (Fig. 11b) over a wide range of temperature. Table 6 compares the performances of the mechanical mixtures at about 250°C. Given that SiO_2 exhibits no deNO_x, the activity reported for the mechanical mixture of Pd(0.89)/CZ and SiO_2 is only due to Pd(0.89)/CZ. It is quite unusual to note that the HSV does not influence the performance of the Pd(0.89)/CZ catalyst as the experiments carried out with 0.10 or 0.20 g of this sample give comparable deNO_x activities (Table 4 and Table 6, Fig. 10d and Fig. 11a). This unexpected result suggests that the geometry of the reactor used in this study was not the best to achieve optimised deNO_x conversions. The deNO_x activity reported for the mechanical mixture made up of Pd(0.93)/SiO_2 and CZ roughly corresponds to the sum of the activities of both catalytic systems. These conclusions are corroborated by the selectivity to N_2 that is: (i) close to that reported for Pd(0.89)/CZ (Table 4) for the mechanical mixture made up of Pd(0.89)/CZ and SiO_2 (Table 6), and (ii) intermediate to those of Pd(0.93)/SiO_2 and CZ (Table 4) for the corresponding mechanical mixture (Table 6).

3.1.13. Steady-state NO-C_3H_6OH-O_2 reaction over $Ce_{0.68}Zr_{0.32}O_2$

Over CZ, C_3H_6 was substituted by 1-C_3H_7OH as reductant. The results of this steady-state experiment are shown in Fig. 12. In contrast to the steady-state measurements with C_3H_6 as reductant (Fig. 10b), CZ exhibits a higher lean deNO_x activity in the presence of 1-C_3H_7OH over a broader range of temperatures than with C_3H_6. In comparison, the highest activity, 19% NO_x to N_2 at 283°C when 1-C_3H_7OH is used as reductant, is more than twice that listed at 361°C with C_3H_6 (Table 4). The selectivity to N_2 in the presence of C_3H_7OH (76%) is comparable to that found in the presence of C_3H_6 (81%).

4. Discussion

4.1. State of Pd in the supported Pd catalysts

The XRD pattern of the calcined Pd(0.93)/SiO_2 sample (Fig. 2) indicates, as expected, the presence of PdO. The corresponding reduced sample exhibits propene hydrogenation activity (Table 1).

As mentioned in the results (part 3.1.3.), due to the overlapping of the diffraction peaks of PdO with those of CZ, XRD characterisation could not be successfully used to investigate the nature of the Pd species of the Pd/CZ catalysts. XANES measurements of oxidised and reduced Pd(0.54)/CZ samples show that they closely resemble those of PdO and the Pd foil, respectively (Fig. 3). As in the case of Pd/SiO_2, these XANES measurements suggest that Pd is present as PdO for the calcined sample (Fig. 3a). Pd/CZ catalysts also catalyse propene hydrogenation (Table 1), which agrees fairly well with the XANES measurements of the reduced Pd(0.54)/CZ sample (Fig. 3), indicating the presence of reduced Pd clusters. Holles and Davis have reported, however, that Pd(4.0)/CeO_x/Al_2O_3 could not be fully reduced even after exposure to CO at 400°C [68]. Comparable conclusions were also

drawn by Matsumara and coworkers for Pd(3.0)/CeO_2 and Pd(2.0)/ZrO_2 samples reduced under H_2 at 300 and 400°C [69,70], respectively. As X-ray absorption spectroscopy is known to provide an average picture of the targeted metal species [71], CO-FTIR measurements were also performed on Pd(0.89)/CZ (Fig. 4b). In agreement with XANES measurements, CO-FTIR spectra recorded after H_2 reduction at 500°C do not reveal the presence of Pd oxidised species, as is the case with a CZ-supported Rh catalyst [58].

The characterisation of these catalysts after oxidising or reducing pretreatments were motivated due to the initial calcination of the samples and the C_3H_6-NO-O_2 TPSR experiment that was carried out before steady-state measurements, the TPSR experiment leading to the exposure of the calcined sample to the C_3H_6 reductant. The characterisation of the Pd/CZ catalysts indicates that Pd is present as PdO in the calcined samples. Nevertheless, one might wonder about the nature of the Pd species in the course of the lean NO_x reaction. Fernàndez-Garcia et al. have recently shown that even under a stoichiometric C_3H_6+CO+NO+O_2 mixture, Pd was not reduced to Pd^0 for Pd(1.0)/$Ce_{0.5}Zr_{0.5}O_2$ up to reaction temperature as high as 400°C, but remained in an oxidised state due to contact between PdO clusters and ceria-zirconia [72]. It is, thus, very likely that the same conclusion also applies to the Pd/CZ catalysts of the present work. This assumption is supported by: (i) the TPR traces revealing greater interaction of the Pd species with CZ than with SiO_2 (Fig. 1), and (ii) the steady-state catalytic results (Table 4 and Table 6) that show markedly different N_2 selectivity for Pd/CZ and Pd/SiO_2 catalysts. The N_2 selectivity found over the Pd/CZ catalysts is, indeed, more than twice that observed over Pd/SiO_2. The N_2 selectivity listed for Pd/SiO_2 agrees well with those already reported over a comparable catalytic system [19], over Pd/Al_2O_3 [34] or over Pt^0 clusters [19]. This means that PdO is reduced to Pd^0 when being supported on SiO_2 even under a lean atmosphere. Such a conclusion has also been reported by Fernàndez-Garcia et al. for alumina-supported Pd catalysts [72]. As already mentioned above, however, these authors

have demonstrated that this was not the case for a Pd(1.0)/$Ce_{0.5}Zr_{0.5}O_2$ catalyst. The obvious higher N_2 selectivity for the Pd/CZ catalysts might also suggest that the deNO_x mechanism occurring over these materials is different from the dissociation mechanism reported over zero-valent PGMs atoms [6,9] and, thus, that the nature of the Pd species of the Pd/CZ catalysts is different from that of Pd^0. These arguments are further supported by the comparison of the light-off of C_3H_6 of the TPSR and reverse TPSR (see part 3.1.10.) that decreases to a significant extent on Pd(0.93)/SiO_2, and it is hardly affected at all on Pd/CZ catalysts. Under the experimental conditions of the present study, it is, therefore, very likely that Pd is present as PdO_x species, with x close to unity [73], rather than Pd^0.

4.2. Lean deNO_x mechanism proposal over PdO_x/CZ catalysts

The results of the present work show that the incorporation of Pd to CZ promotes significantly lean deNO_x activity (Fig. 10). In addition, CZ-supported catalysts exhibit a much higher N_2 selectivity compared with that of Pd^0(0.93)/SiO_2 (Table 4). Centi et al. [31] and Liotta et al. [32] have also recently reported elevated N_2 selectivities over Pt/$Ce_{0.60}Zr_{0.40}O_2$-Al_2O_3 and Pt/$Ce_{0.60}Zr_{0.40}O_2$ catalysts. These authors, however, did not comment about this peculiarity. As already mentioned in the preceding characterisation section, this obvious difference in N_2 selectivity between Pd^0/SiO_2 and PdO_x/CZ catalysts suggests that the lean deNO_x mechanism occurring over PdO_x/CZ catalysts is different from that occurring over Pd^0/SiO_2. The fairly low N_2 selectivity found for Pd^0/SiO_2 (Table 4) indicates that lean deNO_x most likely proceeds through the NO dissociation mechanism [9] on zero-valent Pd clusters, the oxygen left from NO dissociation on the reduced surface being "cleaned" by the C_3H_6 oxidation reaction.

In a recent article [38], we suggested that reaction intermediates such as NO_2, organic nitrogen-containing compounds (RNO_x) and oxygenates ($C_xH_yO_z$) might be involved in the

lean deNO$_x$ catalysis on CZ. In the proposed mechanism, the production of NO_2 and $C_xH_yO_z$, the formation of the latter resulting from the decomposition of R-NO$_x$ intermediates produced by the reaction of NO_2 and C_3H_6, has been assumed to be critical for lean deNO$_x$ activity, as also reported by other authors [34]. The present study also shows that NO oxidation to NO_2 is achieved on the bare support, as the introduction of Pd does not promote such a reaction (Fig. 5). This conclusion is consistent with the work of Krishna et al. in which the authors reported that CeO_2 is a fairly efficient catalyst in the oxidation of NO [74].

The activation of C_3H_6 proceeds unambiguously on the PdO$_x$ catalytic function, as demonstrated by the C_3H_6 light-off temperature that decreases significantly over supported Pd catalysts (Fig. 10 and Table 3). In addition, it is obvious that this low temperature activation of C_3H_6 is responsible for the lean deNO$_x$ activity of PdO$_x$/CZ catalysts, as both C_3H_6 activation and deNO$_x$ occur concomitantly (Fig. 9 and Fig. 10c,d).

One might, however, wonder about the activation process of C_3H_6 in the course of the deNO$_x$ reaction. On that point, the TPD in C_3H_6-O_2 after adsorption of NO-O_2 is very informative. Fig. 7b shows that C_3H_6 is activated through ad-NO_2 species, as already proposed on CZ [38], the low temperature (130-180°C) consumption of C_3H_6 being different from the C_3H_6 profiles observed in the C_3H_6-O_2 reaction on Pd(0.89)/CZ (Fig. 8) and in the TPD in C_3H_6-O_2 after adsorption of NO-O_2 on CZ (Fig. 7a). In this temperature range, it is worthwhile noting that the NO_2 concentration of the TPD in N_2 after adsorption of NO-O_2 on Pd(0.89)/CZ is greater than that of CZ (Fig. 6c, 130-180°C region). These observations strongly suggest that NO_2 species adsorbed on the PdO$_x$ catalytic function account for the activation of C_3H_6. Such a conclusion is also supported by the fact that NO is mainly desorbed in the TPD in C_3H_6-O_2 after adsorption of NO-O_2 (Table 2), whereas NO_2 would have been expected to be the most abundant desorbed compound from the TPD in N_2 (Table 2 and Fig. 6b). As discussed previously [38], the activation of C_3H_6 by ad-NO_2 and the

concomitant release of NO might be attributed to the intermediate formation of R-NO_x compounds, the decomposition of which produces NO and $C_xH_yO_z$.

One might wonder whether lean deNO_x also occurs on the PdO_x catalytic function. Given that lean deNO_x occurs to a significant extent on CZ when C_3H_6 is substituted by 1-C_3H_7OH (Fig. 12), it seems more likely that NO reduction takes place via a lacunar mechanism on reduced CZ sites, as proposed by several groups [75-78]. These authors, indeed, provided evidence for the decomposition of NO to N_2 on prereduced CeO_2 surfaces. It is worth reporting that this decomposition pathway has also been considered in Three-Way Catalysis in which CO is used as reductant [15]. In the course of the lean deNO_x reaction, the creation of the sites responsible for the decomposition of NO would, thus, be achieved by reduction of CZ by the oxygenates ($C_xH_yO_z$) produced by the decomposition of R-NO_x formed on the PdO_x catalytic function.

The corresponding detailed mechanism of the C_3H_6-assisted decomposition of NO on PdO_x/CZ catalysts is described in Fig. 13. This mechanism stresses the key role of NO_2, R-NO_x and $C_xH_yO_z$ as intermediates of the Selective Catalytic Reduction (SCR) of NO_x by hydrocarbons, as also suggested in many studies [34,38 and references therein]. The proposed mechanism is consistent with previous studies of Djega-Mariadassou [16,79] who reported that three catalytic functions were required for the occurrence of the SCR of NO_x by hydrocarbons. In this model, CZ achieves both NO oxidation to NO_2 (cycle 1) and NO decomposition to N_2 (cycle 3), whereas PdO_x activates C_3H_6 via ad-NO_2 species (cycle 2) intermediately producing R-NO_x compounds that further decompose to NO and $C_xH_yO_z$. The role of the latter oxygenates is to reduce CZ to provide the catalytic sites responsible for NO decomposition (catalytic cycle 3). In the proposed mechanism, the reaction of NO_2 with C_3H_6 to give NO back and the competition between the NO oxidation and decomposition reactions on the CZ catalytic sites also account for the limited formation of NO_2 in the course of the

lean $deNO_x$ process (Fig. 7b, Fig. 9 and Fig. 10e). At elevated temperatures, complete oxidation of C_3H_6 by molecular O_2 becomes predominant [80] on PdO_x, and the $deNO_x$ process cannot proceed further.

5. Conclusion

This study shows that the incorporation of Pd to CZ greatly promotes the reduction of NO in the presence of C_3H_6. These catalysts display very stable $deNO_x$ activity even in the presence of 1.7% water, the addition of which induces a reversible deactivation of about 10%.

Ex situ characterisation of the catalysts through propene hydrogenation reaction, XRD, XANES, CO absorption followed by FTIR along with the catalytic results indicate that PdO is reduced to Pd^0 clusters on Pd/SiO_2, this catalyst having been studied as a reference catalyst. This complete reduction process, however, does not occur for PdO_x/CZ catalysts under our experimental conditions.

The PdO_x/CZ catalysts also exhibit much higher selectivity to N_2 than that of Pd^0/SiO_2, the selectivity of which is consistent with those already reported in literature data over supported zero-valent noble metal catalysts. The much higher N_2 selectivity obtained on PdO_x/CZ suggests that the lean $deNO_x$ mechanism occurring on these catalysts is different from that occurring on Pd^0/SiO_2 which consists of the dissociation of NO on reduced palladium sites, followed by the regeneration of the active Pd^0 sites by C_3H_6. The results of the catalytic experiments led us to propose a detailed mechanism (Fig. 13) for which CZ achieves both NO oxidation to NO_2 and NO decomposition to N_2, whereas PdO_x activates C_3H_6 via ad-NO_2 species, intermediately producing R-NO_x compounds that further decompose to NO and $C_xH_yO_z$. The role of the latter oxygenates is to reduce CZ to provide the catalytic sites responsible for NO decomposition. Finally, the proposed C_3H_6-assisted NO

decomposition mechanism stresses the key role of NO_2, R-NO_x and $C_xH_yO_z$ as intermediates of the Selective Catalytic Reduction (SCR) of NO_x by hydrocarbons.

Acknowledgments

Rhodia contributed to part of the financial support for this work; the Ministère de l'Enseignement Supérieur et de la Recherche organization supported the work of Dr. Gorce (Grant 98-4-10713) and Ms Fontaine (Grant 8449-2003). We also thank G. Blanchard for his interest in this work and P. Lavaud for his invaluable help in technical support.

References

[1] K.C. Taylor, in Catalysis Science and Technology, J.R. Anderson, M. Boudart, Automobile Catalytic Converters, Springler-Verlag, Berlin, 1982, p. 119.

[2] M. Shelef, G.W. Graham, Catal. Rev. Sci. Eng. 36 (1994) 431.

[3] M.D. Amiridis, T. Zhang, R.J. Farrauto, App. Catal. B: Env. 10 (1996) 203.

[4] V.I. Pârvulescu, P. Grange, B. Delmon, Catal. Today 46 (1998) 233.

[5] R.J. Farrauto, R.M. Heck, Catal. Today 51 (1999) 351.

[6] R. Burch, J.P. Breen, F.C. Meunier, Appl. Catal. B: Env. 39 (2002) 283.

[7] F. Fajardie, J.-F. Tempère, J.-M. Manoli, O. Touret, G. Blanchard, G. Djéga-Mariadassou, J. Catal. 179 (1998) 469.

[8] T.W. Root, L.D. Schmidt, G.B. Fischer, Surf. Sci. 134 (1983) 30.

[9] R. Burch, P.J. Millington, A.P. Walker, Appl. Catal. B: Env. 4 (1994) 65.

[10] R. Burch, P.K. Loader, N.A. Cruise, Appl. Catal. A: Gen. 147 (1996) 375.

[11] N. Miyoshi, S. Matsumoto, K. Katoh, T. Tanaka, J. Harada, N. Takahashi, K. Yokota, M. Sugiura, K. Kasahara, SAE 950809, 1995.

[12] M. Iwamoto, H. Furukawa, Y. Mina, F. Uemura, S. Mikuriya, S. Kagawa, J. Chem. Soc. Chem. Com. (1986) 1275.

[13] M. Iwamoto, K. Maruyama, N. Yamazoe, T. Seiyama, J. Chem. Soc. Chem. Com. (1966) 615.

[14] Y. Lee, J.N. Armor, App. Catal. 76 (1995) L1.

[15] G. Djéga-Mariadassou, F. Fajardie, J.-F. Tempère, J.-M. Manoli, O. Touret, G. Blanchard, J. Mol. Catal. A: Chem. 161 (2000) 179.

[16] G. Djéga-Mariadassou, Catal. Today 90 (2004) 27.

[17] S. Matsumoto, K. Yokota, H. Doi, M. Kimura, S. Kasahura, Catal. Today 22 (1994) 127.

[18] K. Yogo, M. Umeno, H. Watanabe, E. Kikuchi, Catal. Lett. 19 (1993) 131.

[19] R. Burch, P.J. Millington, Catal. Today 29 (1996) 37.

[20] G.R. Bamwenda, A. Ogata, A. Obuchi, J. Oi, K. Mizuno, J. Skrzypek, Appl. Catal. B: Env. 6 (1995) 311.

[21] J. Li, J. Hao, L. Fu, T. Zhu, Topics Catal. 30/31 (2004) 81.

[22] T. Tanaka, T. Okuhara, M. Misono, Appl. Catal. B: Env. 4 (1994) L1.

[23] R. Burch, T.C. Watling, Catal Lett. 37 (1996) 51.

[24] R. Burch, T.C. Watling, Catal Lett. 43 (1997) 19.

[25] T. Okuhara, Y. Hasada, M. Misono, Catal. Today 35 (1997) 83.

[26] R. Burch, T.C. Watling, Appl. Catal. B: Env. 11 (1997) 207.

[27] R. Burch, J.A. Sullivan, T.C. Watling, Catal. Today 42 (1998) 13.

[28] E. Joubert, T. Bertin, J.C. Ménézo, J. Barbier, Appl. Catal. B: Env. 23 (1999) L83.

[29] D.K. Captain, K.L. Roberts, M.D. Amiridis, Catal. Today 42 (1998) 93.

[30] P. Denton, A. Giroir-Fendler, H. Praliaud, M. Primet, J. Catal. 189 (2000) 410.

[31] G. Centi, P. Fornasiero, M. Graziani, J. Kašpar, F. Vazzana, Topics Catal. 16/17 (2001) 157.

[32] L.F. Liotta, A. Longo, A. Macaluso, A. Martorana, G. Pantaleo, A.M. Venezia, G. Deganello, Appl. Catal. B: Env. 48 (2004) 133.

[33] A. Obuchi, A. Ogata, H. Takahashi, J. Oi, G.R. Bamwenda, K. Mizuno, Catal. Today 29 (1996) 103.

[34] K.O. Haj, S. Ziyade, M. Ziyad, F. Garin, Appl. Catal. B: Env. 37 (2002) 49.

[35] Y. Traa, B. Burger, J. Weitkamp, J. Chem. Soc. Chem. Comm. 21 (1999) 2187.

[36] P. Degobert, Automobiles and Pollution (Institut Français du Pétrole Publications, Editions Technip, Paris 1995)

[37] S.N. Orlik, V.L. Struzhko, T.V. Mironyuk, G.M. Tel'biz, Theor. Exp. Chem. 37 (2001) 311.

[38] O. Gorce, F. Baudin, C. Thomas, P. Da Costa, G. Djéga-Mariadassou, Appl. Catal. B: Env. 54 (2004) 69.

[39] R. Rajasree, J.H.B.J. Hoebink, J.C. Shouten, J. Catal. 223 (2004) 36.

[40] N. Hickey, P. Fornasiero, R. Di Monte, J. Kašpar, J.R. González-Velasco, M.A. Gutiérrez-Ortiz, M.P. González-Marcos, J.M. Gatica, S. Bernal, J. Chem. Soc., Chem. Commun. (2004) 196.

[41] S. Bedrane, C. Descorme, D. Duprez, Catal. Today 75 (2002) 41.

[42] S. Salasc, V. Perrichon, M. Primet, N. Mouaddib-Moral, J. Catal. 206 (2002) 82.

[43] A. Iglesia-Juez, A. Martínez-Arias, M. Fernández-García, J. Catal. 221 (2004) 148.

[44] C. Bozo, N. Guilhaume, J.-M. Herrmann, J. Catal. 203 (2001) 393.

[45] G. Pecchi, P. Reyes, R. Zamora, T. Lopez, R. Gomez, J. Chem. Tech. Biotech. 80 (2005) 268.

[46] J. Breen, R. Burch, H.M. Coleman, Appl. Catal. B: Env. 39 (2002) 65.

[47] S.H. Overbury, D.R. Mullins, in Catalyis by Ceria and Related Materials, A. Trovarelli (Ed.), Ceria Surfaces and Films for Model Catalytic Studies Using Surface Analysis Techniques, Imperial College Press, London, 2002, p.328.

[48] L. Salin, C. Potvin, J.-F. Tempère, M. Boudart, G. Djéga-Mariadassou and J.-M. Bart, Ind. Eng. Chem. Res. 37 (1998) 4531.

[49] A. Michalowicz, Logiciels pour la chimie; Société Française de Chimie, Paris (1991) 102.

[50] A. Michalowicz, J. Phys. IV France 7 (1997) 235.

[51] C. de Leitenburg, A. Trovarelli, J. Kašpar, J. Catal. 166 (1997) 98.

[52] H.-W. Jen, G.W. Graham, W. Chun, R.W. McCabe, J.-P. Cuif, S.E. Deutsch, O. Touret, Catal. Today 50 (1999) 309.

[53] R. Di Monte, P. Fornasiero, M. Graziani, J. Kašpar, J. Alloys Comp. 275-277 (1998) 877.

[54] P. Fornasiero, N. Hickey, J. Kašpar, T. Montini, M. Graziani, J. Catal. 189 (2000) 339.

[55] P. Fornasiero, J. Kašpar, M. Graziani, J. Catal. 167 (1997) 576.

[56] M.-F. Luo, X.-M. Zheng, Appl. Catal. A: General 189 (1999) 15.

[57] P. Fornasiero, R. Di Monte, G. Ranga Rao, J. Kašpar, S. Meriani, A. Trovarelli, M. Graziani, J. Catal. 151 (1995) 168.

[58] C. Fontaine, C. Thomas, J.-M. Krafft, O. Gorce, F. Villain, G. Djéga-Mariadassou, *in preparation.*

[59] K. Hadjiivanov, G.N. Vayssilov, Adv. Catal. 47 (2002) 307.

[60] J.-C. Lavalley, J. Saussey, J. Lamotte, R. Breault, J. P. Hindermann, A. Kiennemann, J. Phys. Chem. 94 (1990) 5941.

[61] A. Badri, C. Binet, J.-C. Lavalley, J. Phys. Chem. 100 (1996) 8363.

[62] A. Badri, C. Binet, J.-C. Lavalley, J. Chem. Soc., Farad. Trans. 92 (1996) 1603.

[63] A. Bensalem, J.-C. Muller, D. Tessier, F. Bozon-Verduraz, J. Chem. Soc., Farad. Trans. 92 (1996) 3233.

[64] C. Force, J. P. Belzunegui, J. Sanz, A. Martínez-Arias, J. Soria, J. Catal. 197 (2001) 192.

[65] K.I. Choi, M.A. Vannice, J. Catal. 127 (1991) 465.

[66] L. Sordelli, G. Matra, R. Psaro, S. Coluccia, J. Chem. Soc., Dalton Trans. 5 (1996) 765.

[67] M. Ogura, M. Hayashi, S. Kage, M. Matsukata, E. Kikuchi, Appl. Catal. B: Env. 23 (1999) 247.

[68] J.H. Holles, R.J. Davis, J. Phys. Chem. B 104 (2000) 9653.

[69] W-J. Shen, Y. Ichihashi, M. Okumara, Y. Matsumara, Catal. Lett. 64 (2000) 23.

[70] Y. Matsumara, M. Okumara, Y. Usami, K. Kagawa, H. Yamashita, M. Anpo, M. Haruta, Catal. Lett. 44 (1997) 189.

[71] M. Vaarkamp, D.C. Koningsberger, in G. Ertl, H. Knözinger, J. Weitkamp (Ed.), Handbook of Heterogeneous Catalysis, Wiley-VCH, Weinheim, 1997, Vol. 2, p. 475.

[72] M. Fernàndez-Garcia, A. Iglesia-Juez, A. Martínez-Arias, A.B. Hungría, J.A. Anderson, J.C. Conesa, J. Soria, J. Catal. 221 (2004) 594.

[73] T. Maillet, C. Solleau, J. Barbier Jr., D. Duprez, Appl. Catal. B: Env. 14 (1997) 85.

[74] K. Krishna, M. Makkee, Appl. Catal. B: Env. 59 (2005) 35.

[75] M. Niwa, Y. Furukawa, Y. Murakami, J. Coll. Int. Sci. 86 (1982) 260.

[76] A. Martinez-Arias, J. Soria, J.C. Conesa, X.L. Soane, A. Arcoya, R. Cataluna, J. Chem. Soc. Faraday. Trans. 91 (1995) 1679.

[77] S.H. Overbury, D.R. Mullins, D.R. Huntley, Lj. Kundakovic, J. Catal. 186 (1999) 296.

[78] M. Daturi, N. Bion, J. Saussey, J.-C. Lavalley, C. Hedouin, T. Seguelon, G. Blanchard, Phys. Chem. Chem. Phys. 3 (2001) 252.

[79] G. Djéga-Mariadassou, M. Boudart, J. Catal. 216 (2003) 89.

[80] J. Haber, W. Turek, J. Catal. 190 (2000) 320.

Table 1: Determination of the percentage of exposed zero-valent Pd atoms (PEM^0) over $Ce_{0.68}Zr_{0.32}O_2$ (CZ)- and silica-supported catalysts by means of propene hydrogenation reactions [48].

Catalysts	Pd(0.54)/CZ	Pd(0.89)/CZ	Pd(0.93)/SiO_2
Pd^0 (%)	17	16	22

Table 2: Amounts of adsorbed or desorbed NO_x (NO+ NO_2) and desorbed N_2O in the course of the TPD experiments after exposure of the catalysts to NO-O_2 (340 ppm – 8%) in N_2

		Amounts of adsorbed (ads.) or desorbed (des.) species (10^{-5} mol g^{-1})					
Catalysts	experiment	$NO_{x\ ads.}$	$NO_{des.}$	$NO_{2\ des.}$	$NO_{x\ des.}$	$N_2O_{\ des.}$	N balance*
$Ce_{0.68}\ Zr_{0.32}O_2$ (CZ)	TPD in N_2	54.8	8.1	46.5	54.6	0.0	0.1
	TPD in C_3H_6-O_2	48.2	19.0	7.8	26.8	5.8	4.9
Pd(0.89)/CZ	TPD in N_2	47.6	6.2	36.4	42.7	0.0	2.5
	TPD in C_3H_6-O_2	51.8	20.3	5.1	25.4	5.4	7.8

* N balance calculated with respect to N_2 equivalent

Table 3: C_3H_6 light-off temperatures (°C) of $Ce_{0.68}Zr_{0.32}O_2$ (CZ)- and silica-supported catalysts; 340ppm NO, 8% O_2, 1900 ppm C_3H_6 and N_2 balance

	Ads NO-O_2 TPD in O_2-C_3H_6	Transient O_2-C_3H_6	Transient NO-O_2-C_3H_6	Steady-state NO-O_2-C_3H_6
CZ	450	473	387	380
Pd(0.54)/CZ	-	277	276	303
Pd(0.89)/CZ	276	251	252	243
Pd(0.93)/SiO_2	-	-	298*	-
		236	237	237

* Light-off temperature measured in the course of the first NO-O_2-C_3H_6 TPSR

Table 4: Temperature of maximum of N_2 formation and percentage of NO_x converted to N_2 at this temperature over $Ce_{0.68}Zr_{0.32}O_2$ (CZ)-and silica-supported catalysts for the steady-state $NO-O_2-C_3H_6$ reaction (340 ppm - 8 % -1900 ppm, N_2 balance)

Catalysts	CZ	Pd(0.54)/CZ	Pd(0.89)/CZ	Pd(0.93)/SiO_2
Sample Weight (g)	0.20	0.20	0.20	0.07
T max N_2 (°C)	361	263	243	243
Conversion of NO_x to N_2 (%)	8	21	29	7
Selectivity to N_2 (%)*	81	83	87	28
C_3H_6 conversion (%)	34	38	50	58

* Selectivity to N_2 referred to as (N_2/(N_2 + N_2O) x 100)

Table 5: Influence of the addition of 1.7% water on the conversions of C_3H_6 and NO_x to N_2 at 278°C in the course of the C_3H_6-NO-O_2 reaction (1900 ppm- 340 ppm – 8 %, balance N_2) versus time on stream on Pd(0.89)/$Ce_{0.68}Zr_{0.32}O_2$.

	Time on stream (h)			
	0	1	20	20.5
H_2O (%)	0	1.7	1.7	0
Conversion of NO_x to N_2 (%)	27	24	25	29
Selectivity to N_2 (%)*	75	76	76	77
C_3H_6 conversion (%)	65	62	62	60

* Selectivity to N_2 referred to as (N_2/(N_2 + N_2O) x 100)

Table 6: Percentage of NO_x converted to N_2 over $Ce_{0.68}Zr_{0.32}O_2$ (CZ)-and silica-supported catalysts for the steady-state $NO-O_2-C_3H_6$ reaction (340 ppm- 8 % -1900 ppm, N_2 balance)

Catalysts	Pd(0.89)/CZ + SiO_2	Pd(0.93)/SiO_2 + CZ
Sample Weight (g)	0.10 + 0.10	0.10 + 0.10
T (°C)	250	255
Conversion of NO_x to N_2 (%)	29	12
Selectivity to N_2 (%)*	86	51
C_3H_6 conversion (%)	47	50

* Selectivity to N_2 referred to as (N_2/(N_2 + N_2O) x 100)

Figure captions

Fig. 1: Temperature-Programmed Reduction profiles of the calcined (air 500°C, 2h) catalysts.

Fig. 2: XRD patterns of SiO_2, Pd(0.93)/SiO_2 and $Ce_{0.68}Zr_{0.32}O_2$.

Fig. 3: XANES spectra at the Pd K edge for PdO (▲), the Pd foil (Δ) and Pd(0.54)/CZ (oxidized in air at 500°C: ---- or reduced in H_2 at 500°C: —).

Fig. 4: FT infrared spectra of (a) $Ce_{0.68}Zr_{0.32}O_2$ (CZ) and (b) Pd(0.89)/CZ, reduced under flowing H_2 at 500°C for 2h and evacuation at 500°C for 1h, after introduction of equilibrated pressures of 0.9 (---) and 18 (—) torr of CO.

Fig. 5: Steady-state catalytic conversion of NO oxidation to NO_2 in the course of the NO-O_2 reaction (340 ppm - 8%, balance N_2): (♦) $Ce_{0.68}Zr_{0.32}O_2$ (CZ), (●) Pd(0.54)/CZ.

Fig. 6: NO_x Temperature-Programmed Desorption profiles in N_2 after exposure of the catalysts to NO-O_2 (340 ppm - 8%, balance N_2) at RT: (a) $Ce_{0.68}Zr_{0.32}O_2$ (CZ), (b) Pd(0.89)/CZ and (c) their comparison, the NO_x TPD of Pd(0.89)/CZ having been normalised with respect to the amount of NO_x adsorbed on CZ (Table 2).

Fig. 7: Temperature-Programmed Desorption profiles in C_3H_6-O_2 (1900 ppm – 8%O_2, balance N_2) after exposure of the catalysts to NO-O_2 (340 ppm - 8%, balance N_2), at RT: (a) $Ce_{0.68}Zr_{0.32}O_2$ (CZ), (b) Pd(0.89)/CZ.

Fig. 8: Transient C_3H_6-O_2 (1900 ppm - 8% O_2, balance N_2) reaction over Pd(0.93)/SiO_2 and Pd(0.89)/$Ce_{0.68}Zr_{0.32}O_2$.

Fig. 9: Temperature-Programmed Surface Reaction profiles of C_3H_6-NO-O_2 (1900 ppm - 340 ppm-8%) after exposure of Pd(0.89)/$Ce_{0.68}Zr_{0.32}O_2$ to C_3H_6-NO-O_2 (1900 ppm - 340 ppm - 8%, balance N_2) at RT.

Fig. 10: Steady-state catalytic conversions of C_3H_6 and NO_x to N_2 in the course of the C_3H_6-NO-O_2 reaction (1900 ppm- 340 ppm - 8%, balance N_2): (a) Pd(0.93)/SiO_2 (0.07g), (b) $Ce_{0.68}Zr_{0.32}O_2$ (CZ, 0.20g), (c) Pd(0.54)/CZ (0.20g), (d) Pd(0.89)/CZ (0.20g), and of NO to NO_2 over Pd(0.54)/CZ (0.20g) (e): (●) NO-O_2 reaction (340 ppm - 8%, balance N_2), (○) C_3H_6-NO-O_2 reaction (1900 ppm- 340 ppm - 8%, balance N_2).

Fig. 11: Steady-state catalytic conversions of C_3H_6 and NO_x to N_2 in the course of the C_3H_6-NO-O_2 reaction (1900 ppm- 340 ppm - 8%, balance N_2) of mechanical mixtures: (a) Pd(0.89)/$Ce_{0.68}Zr_{0.32}O_2$ + SiO_2 (0.10g + 0.10g), (b) Pd(0.93)/ SiO_2 + $Ce_{0.68}Zr_{0.32}O_2$ (0.10g + 0.10g)

Fig. 12: Steady-state catalytic conversions of C_3H_7OH and NO_x to N_2 in the course of the C_3H_7OH-NO-O_2 reaction (2200 ppm- 340 ppm - 8%, balance N_2) over $Ce_{0.68}Zr_{0.32}O_2$ (CZ).

Fig. 13: (a) Schematic representation of the catalytic functions, (b) Mechanism of the lean C_3H_6-assisted decomposition of NO over Pd/$Ce_{0.68}Zr_{0.32}O_2$ (CZ) catalysts, $\boxed{O}$, R-NO_x, $C_xH_yO_z$ representing an oxygen from the surface of the CZ support, organic nitrogen-containing and oxygenates compounds of undefined composition, respectively.

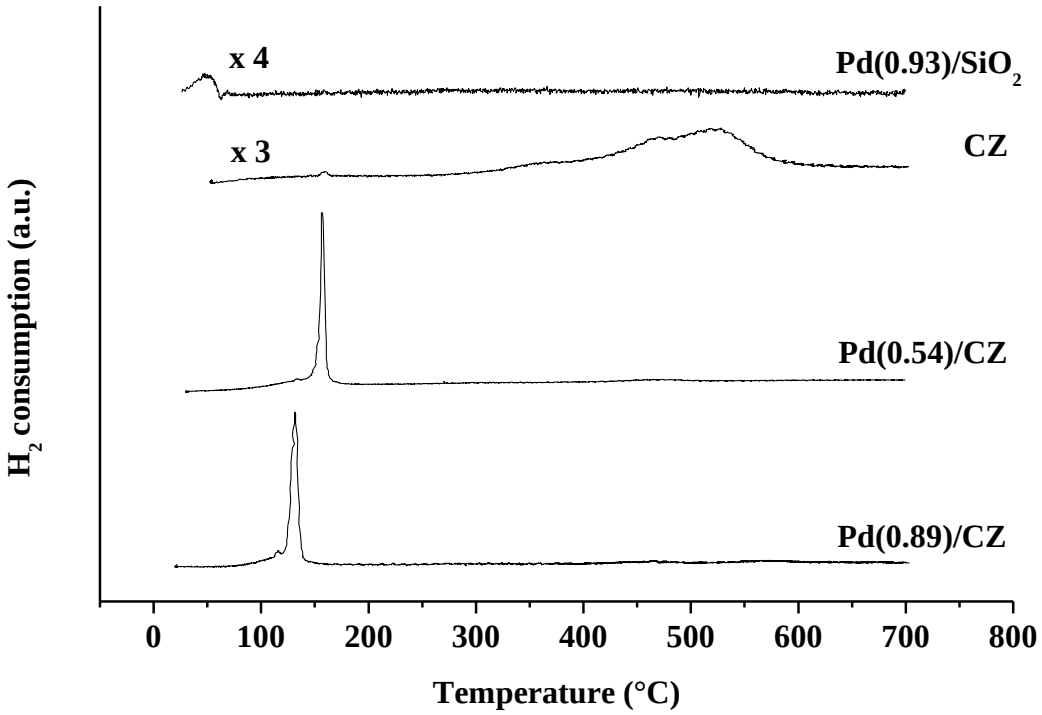
x 4
Pd(0.93)/SiO2
x 3
CZ
Pd(0.54)/CZ
Pd(0.89)/CZ
H2 consumption (a.u.)
0
100
200
300
400
500
600
700
800
Temperature (°C)

Fig. 1

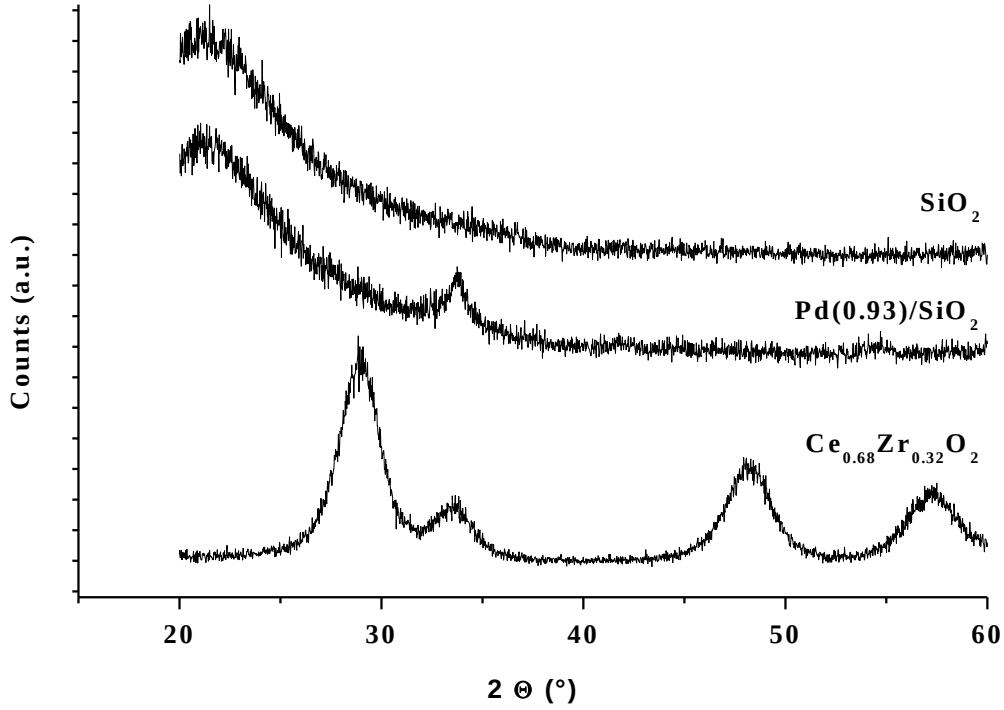

Fig. 2

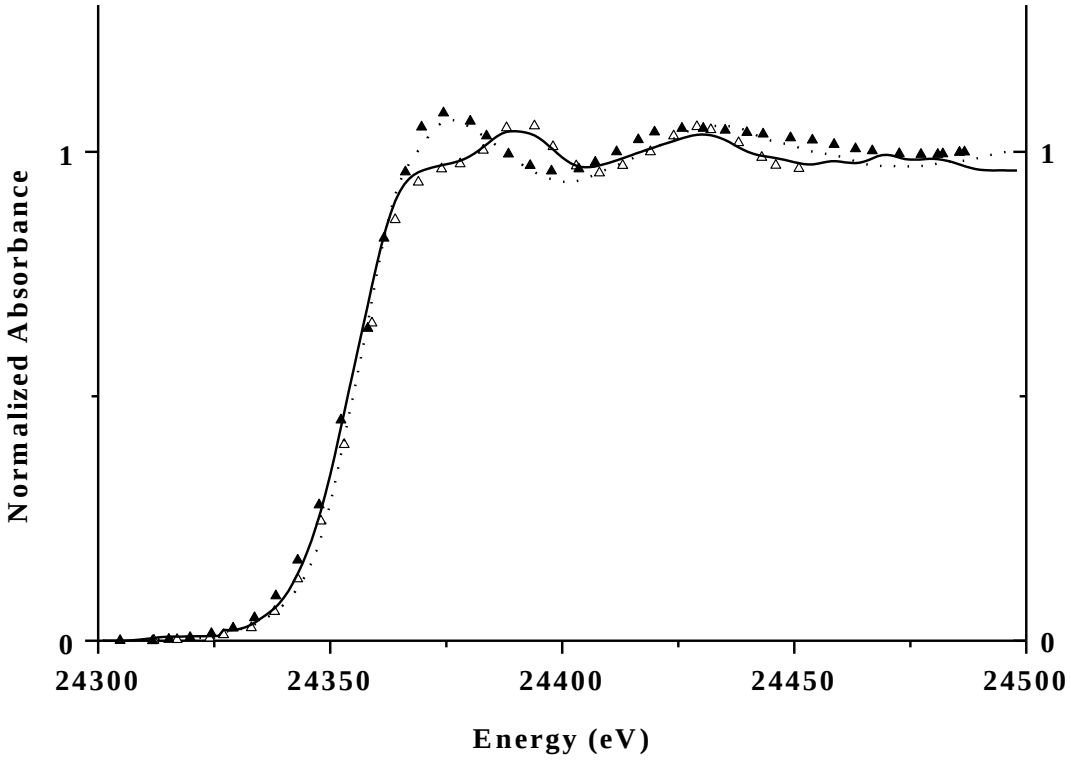
Normalized Absorbance
1
0
1
0
24300
24350
24400
24450
24500
Energy (eV)

Fig. 3

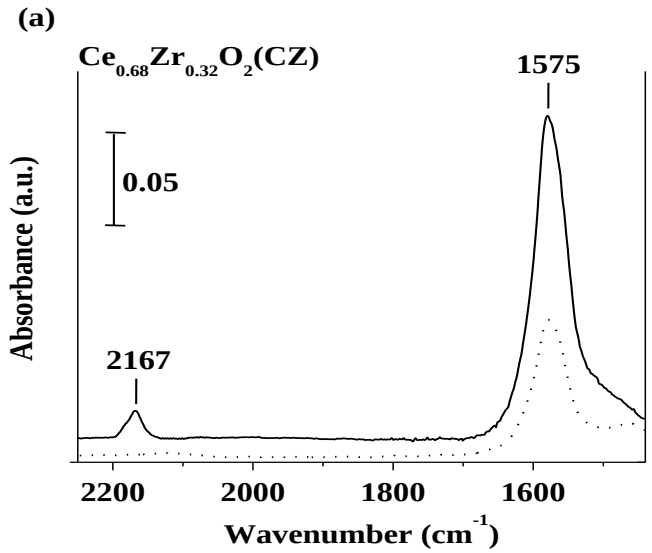
(a)
Ce0.68Zr0.32O2(CZ)
1575
0.05
2167
Absorbance (a.u.)
2200
2000
1800
1600
Wavenumber (cm-1)

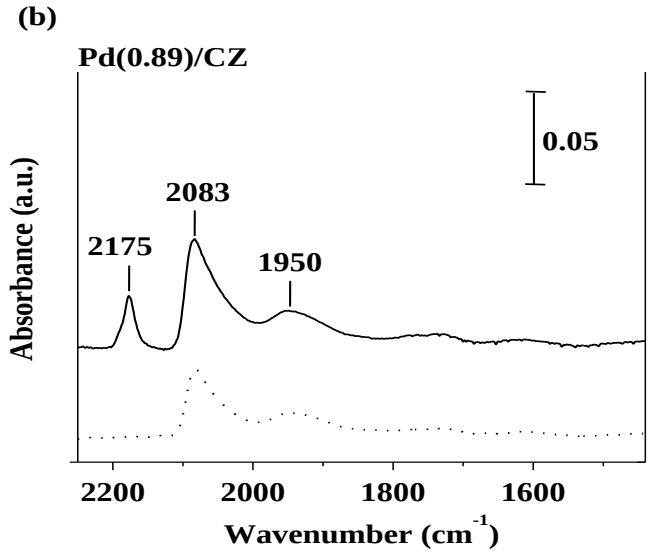
(b)
Pd(0.89)/CZ
0.05
2083
2175
1950
Absorbance (a.u.)
2200
2000
1800
1600
Wavenumber (cm-1)

Fig. 4

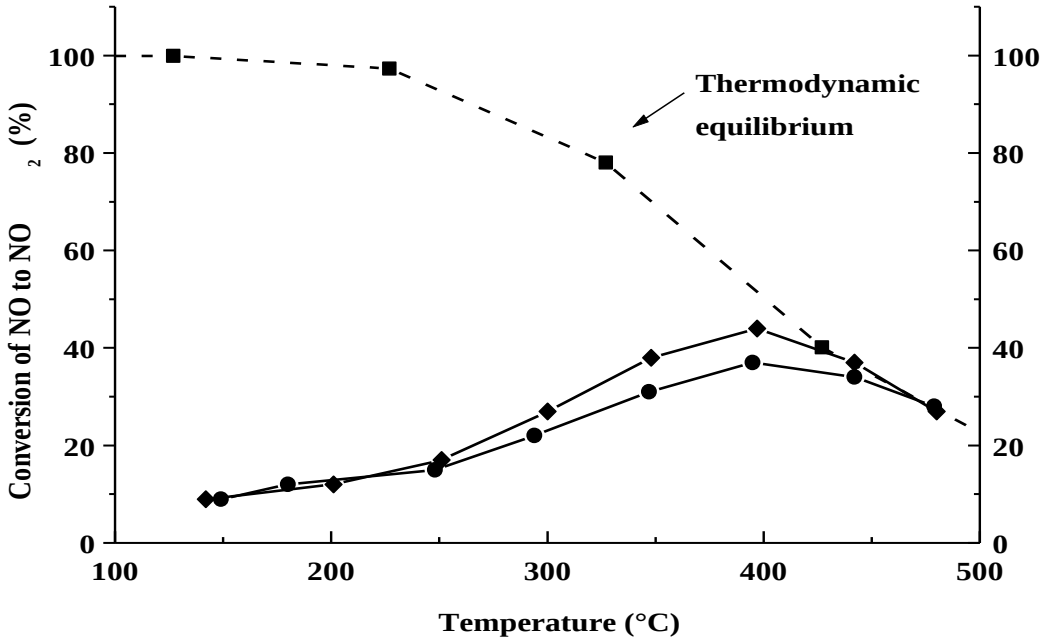
Thermodynamic
equilibrium
Conversion of NO to NO 2 (%)
Temperature (°C)
0
20
40
60
80
100
100
200
300
400
500

Fig. 5

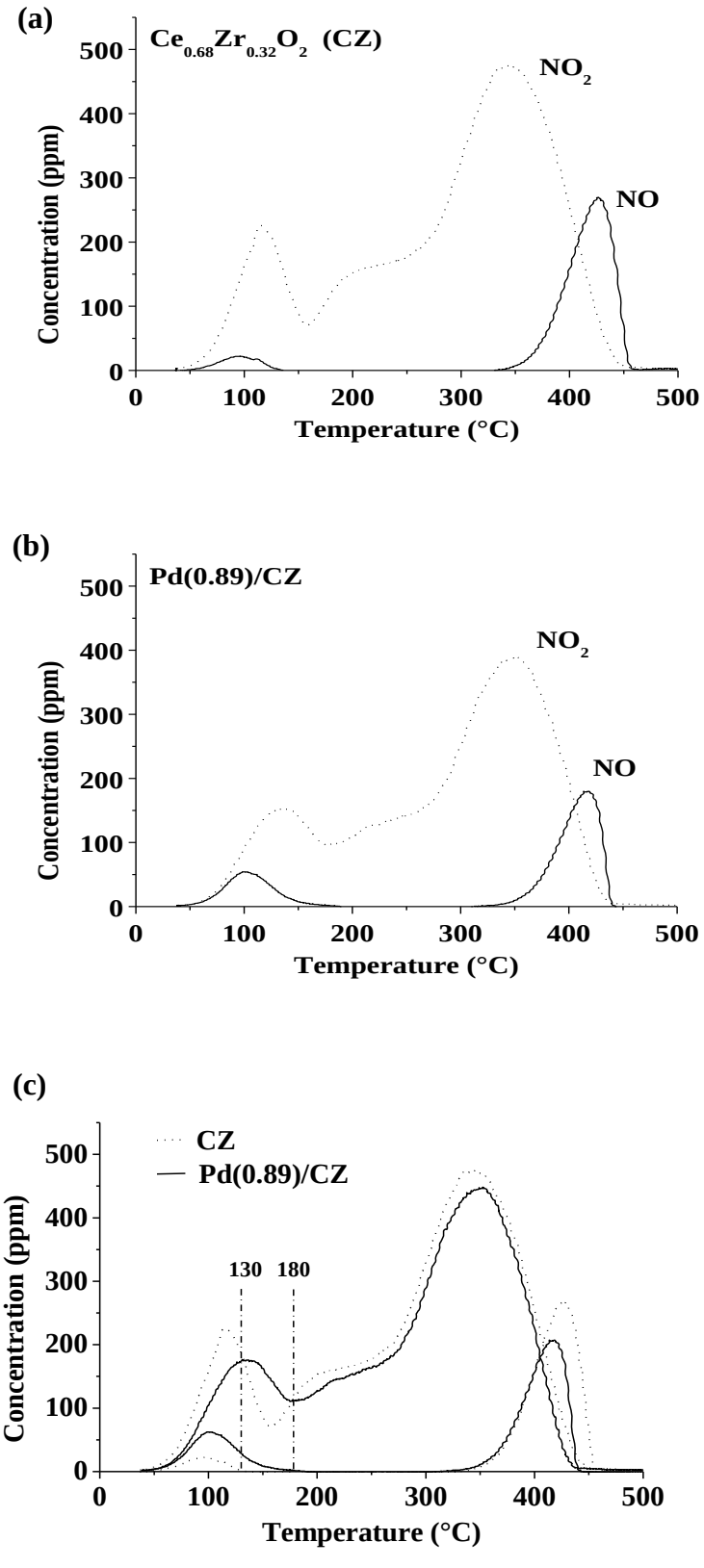
(a)
Ce0.68Zr0.32O2 (CZ)
NO2
NO
Concentration (ppm)
Temperature (°C)
(b)
Pd(0.89)/CZ
NO2
NO
Concentration (ppm)
Temperature (°C)
(c)
CZ
Pd(0.89)/CZ
130
180
Concentration (ppm)
Temperature (°C)

Fig. 6

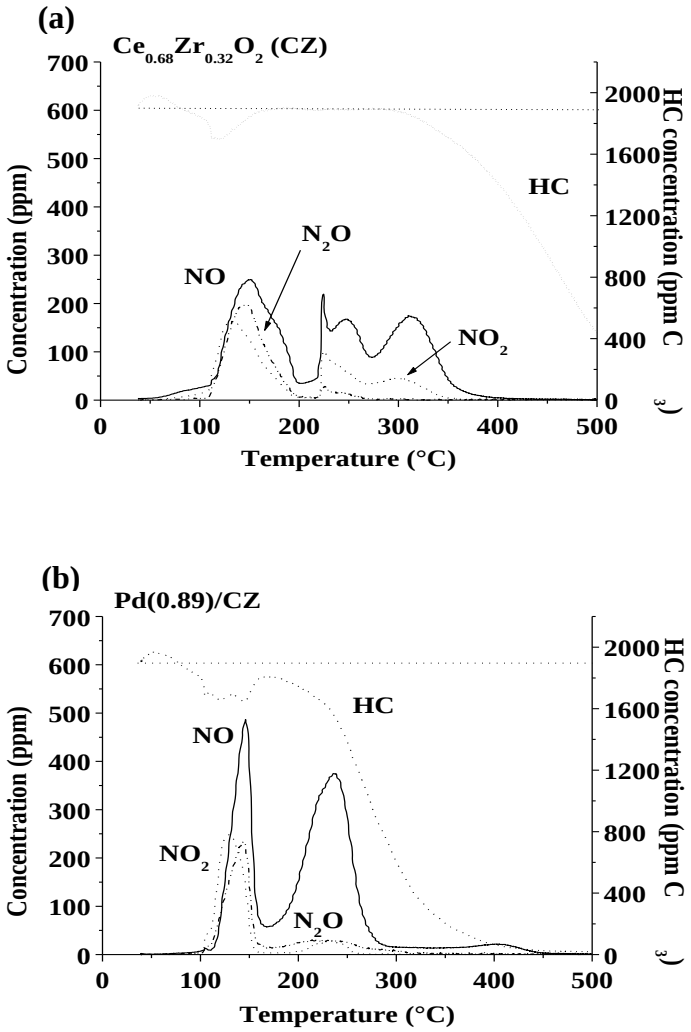
(a)
Ce0.68Zr0.32O2 (CZ)
Concentration (ppm)
HC concentration (ppm C3)
Temperature (°C)
HC
N2O
NO
NO2
(b)
Pd(0.89)/CZ
Concentration (ppm)
HC concentration (ppm C3)
Temperature (°C)
HC
NO
NO2
N2O

Fig. 7

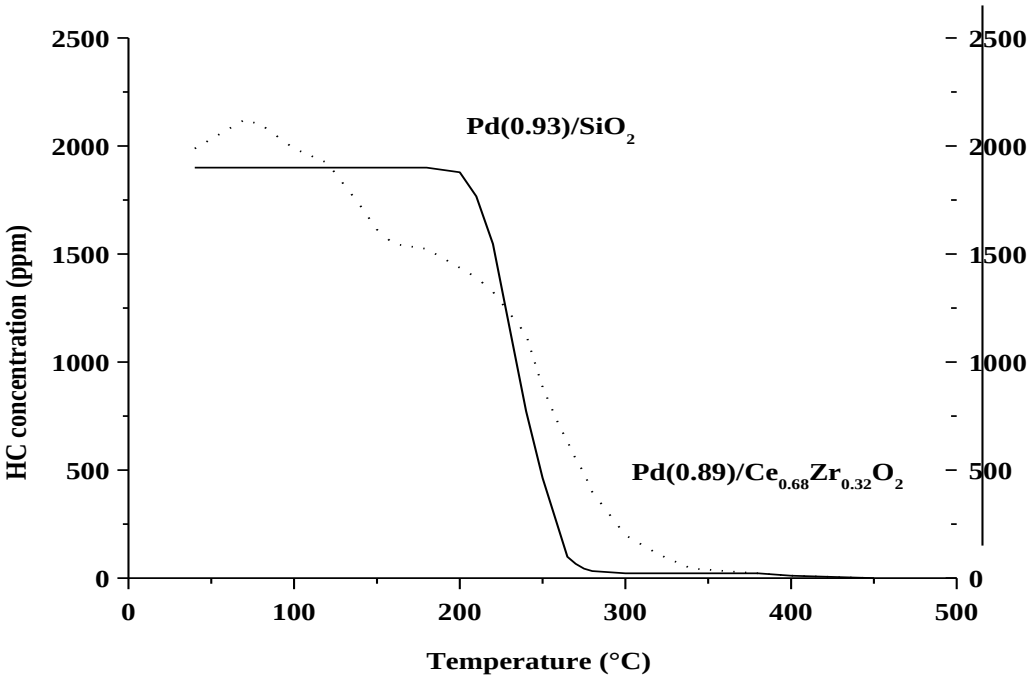
HC concentration (ppm)
Temperature (°C)
Pd(0.93)/SiO2
Pd(0.89)/Ce0.68Zr0.32O2
0
500
1000
1500
2000
2500
0
100
200
300
400
500

Fig. 8

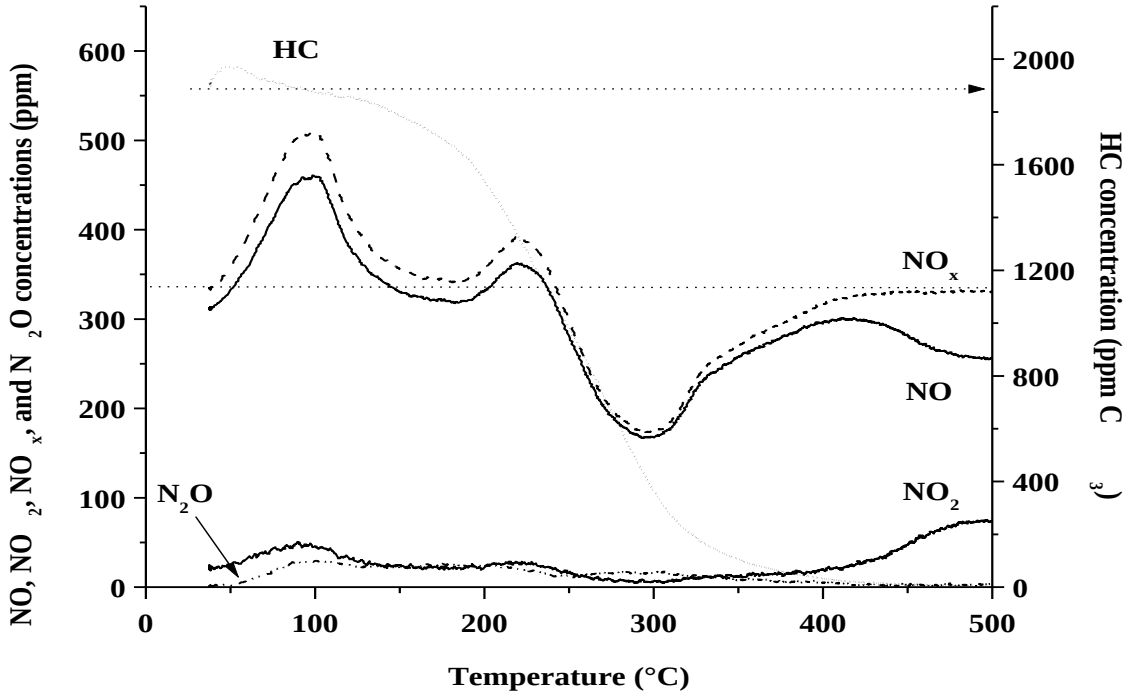
HC
NO$_x$
NO
NO$_2$
N$_2$O
NO, NO$_2$, NO$_x$, and N$_2$O concentrations (ppm)
HC concentration (ppm C$_3$)
Temperature (°C)
0
100
200
300
400
500
600
2000
1600
1200
800
400

Fig. 9

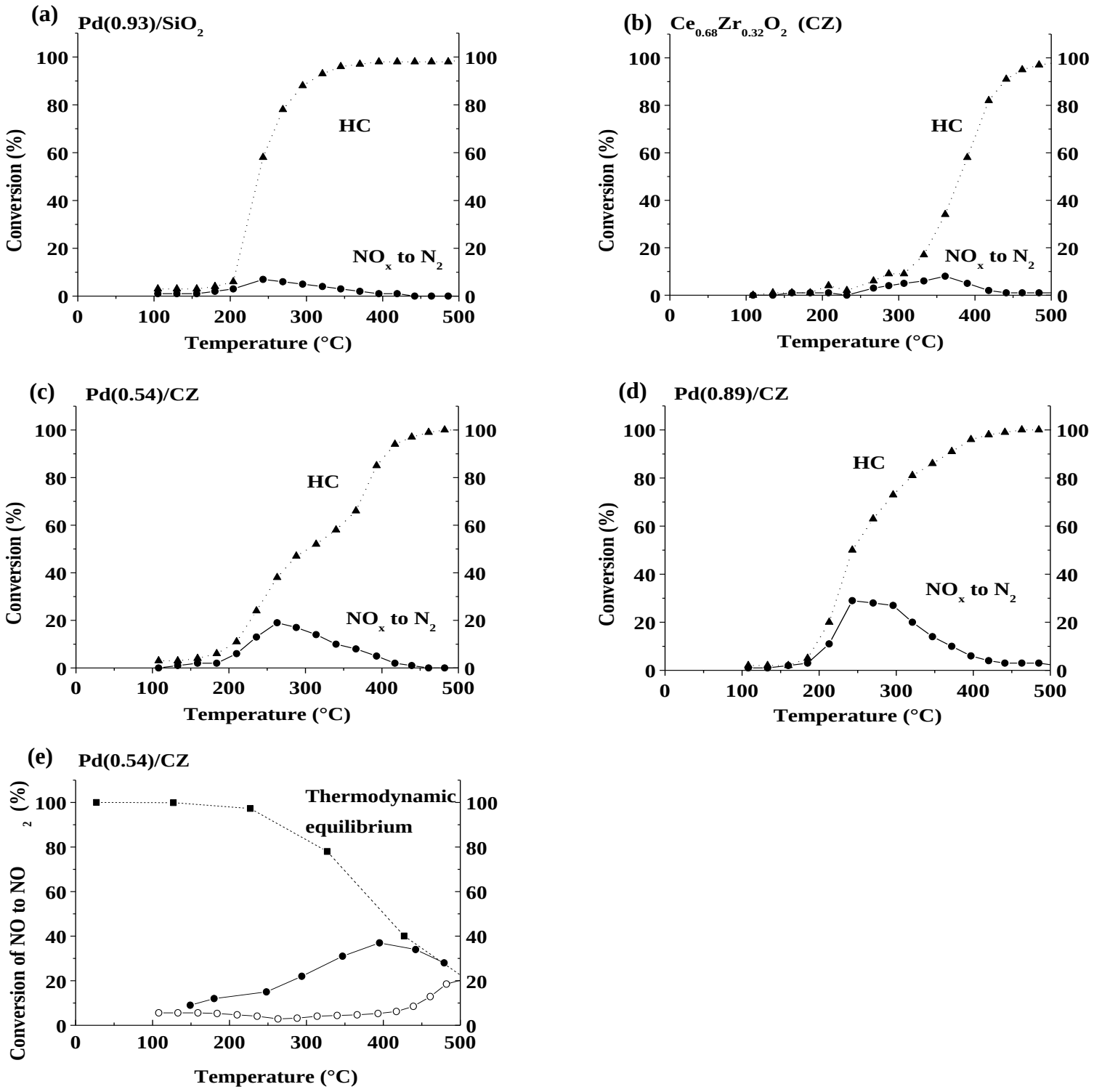
(a)
Pd(0.93)/SiO2
HC
NOx to N2
Conversion (%)
Temperature (°C)
(b)
Ce0.68Zr0.32O2 (CZ)
HC
NOx to N2
Conversion (%)
Temperature (°C)
(c)
Pd(0.54)/CZ
HC
NOx to N2
Conversion (%)
Temperature (°C)
(d)
Pd(0.89)/CZ
HC
NOx to N2
Conversion (%)
Temperature (°C)
(e)
Pd(0.54)/CZ
Thermodynamic equilibrium
Conversion of NO to NO2 (%)
Temperature (°C)

Fig. 10

(a)

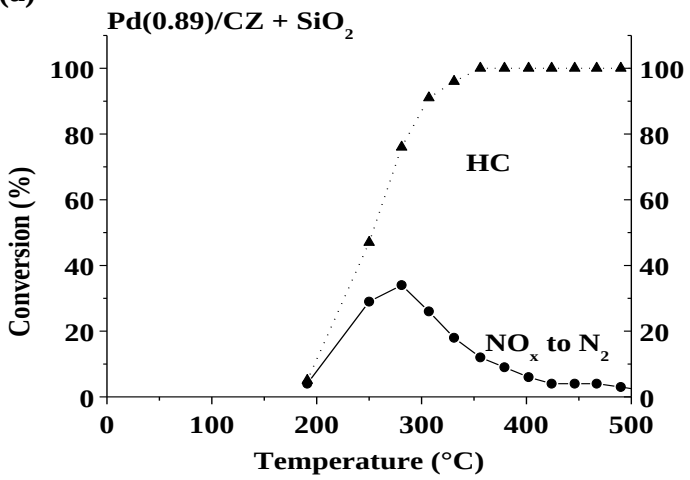
Pd(0.89)/CZ + SiO2
Conversion (%)
Temperature (°C)
HC
NOx to N2
0
20
40
60
80
100
0
100
200
300
400
500

(b)

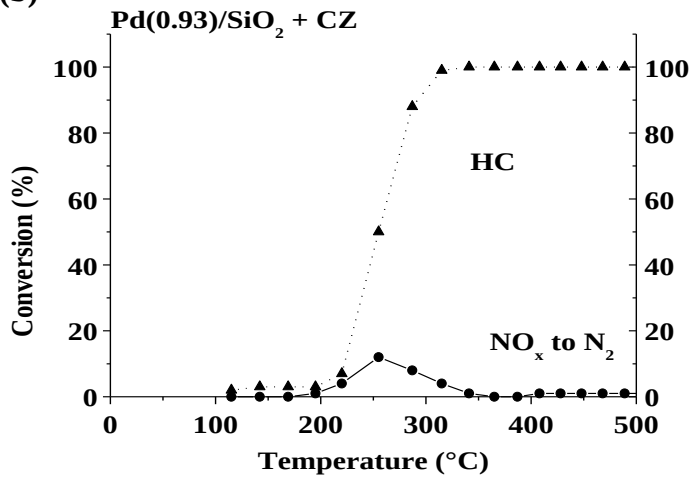
Pd(0.93)/SiO2 + CZ
Conversion (%)
Temperature (°C)
HC
NOx to N2
0
20
40
60
80
100
0
100
200
300
400
500

Fig. 11

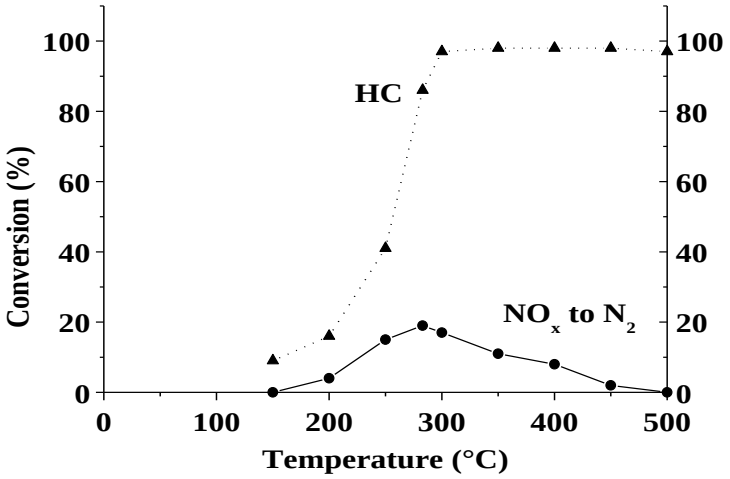
Conversion (%)
Temperature (°C)
HC
NO$_x$ to N$_2$
0
20
40
60
80
100
0
100
200
300
400
500

Fig. 12

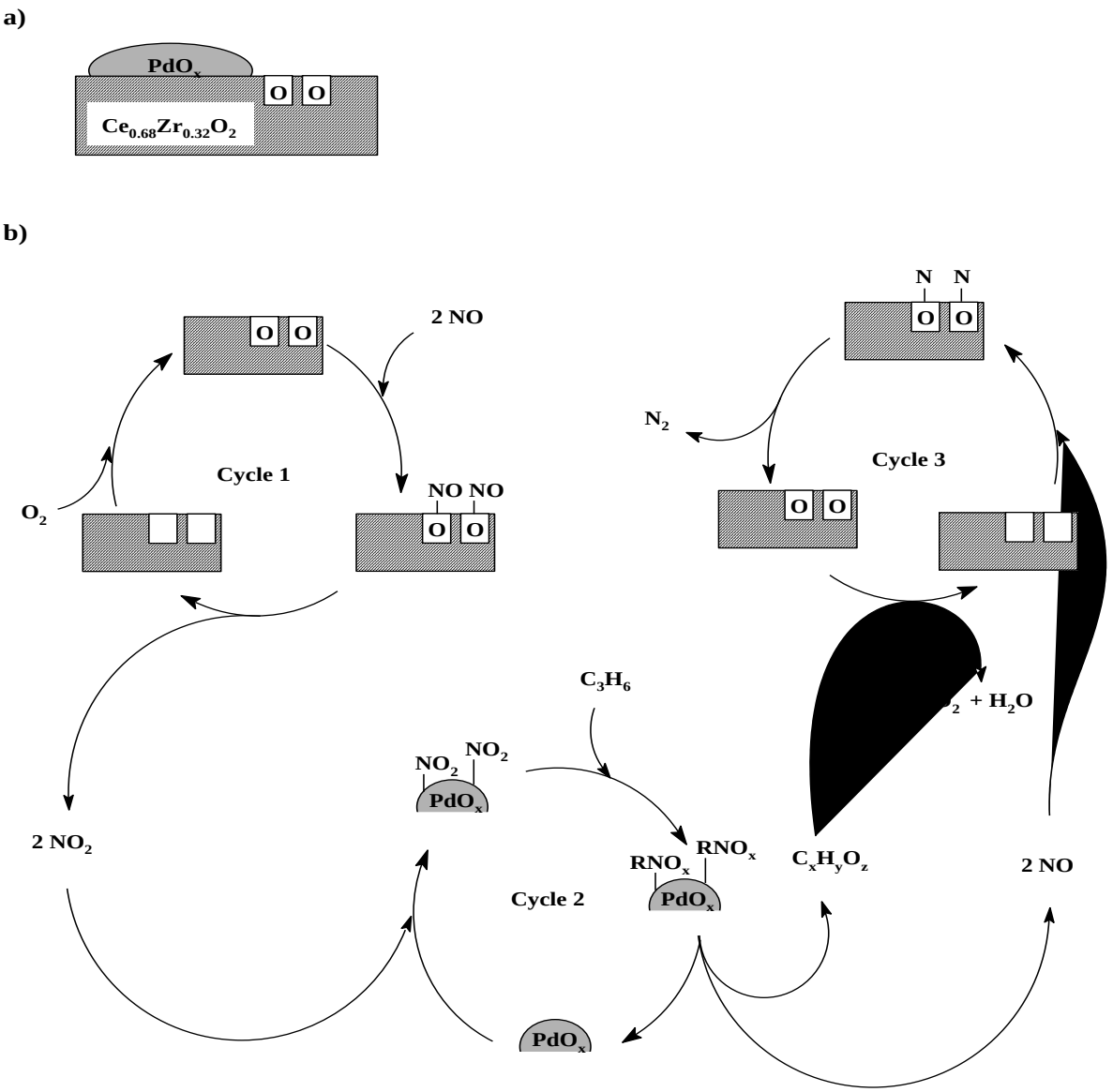
a)
PdOx
O O
Ce0.68Zr0.32O2
b)
2 NO
O O
Cycle 1
O2
NO NO
O O
2 NO2
N N
O O
N2
Cycle 3
O O
C3H6
NO2 NO2
PdOx
RNOx RNOx
PdOx
Cycle 2
CxHyOz
+ H2O
2 NO
PdOx

Fig. 13